NACA TN 3339

NATIONAL ADVISORY COMMITTEE FOR AERONAUTICS

TECHNICAL NOTE 3339

EXPERIMENTS ON TURBULENT FLOW THROUGH CHANNELS HAVING POROUS ROUGH SURFACES WITH OR WITHOUT AIR INJECTION

By E. R. G. Eckert, Anthony J. Diaguila, and Patrick L. Donoughe

Lewis Flight Propulsion Laboratory
Cleveland, Ohio

Washington
February 1955

NATIONAL ADVISORY COMMITTEE FOR AERONAUTICS

TECHNICAL NOTE 3339

EXPERIMENTS ON TURBULENT FLOW THROUGH CHANNELS HAVING POROUS ROUGH SURFACES WITH OR WITHOUT AIR INJECTION

By E. R. G. Eckert, Anthony J. Diaguila, and Patrick L. Donoughe

SUMMARY

Transpiration cooling, obtained by injecting a coolant through a porous surface, is receiving increased consideration as an effective means of maintaining walls exposed to a hot gas stream at temperatures that can be tolerated by the material. Applications for which this cooling method is considered are the cooling of different structural elements such as turbine blades or the walls of combustion chambers in jet engines and parts of the skin of missiles. In some of these applications the surface roughness inherently connected with a porous material may exceed the limit for which such a surface is considered as hydraulically smooth.

In order to obtain information on friction and flow characteristics of rough surfaces under the condition of fluid injection, an investigation with turbulent air flow was made in a rectangular channel. Provisions were made so that porous samples with varying degrees of roughness could be installed in the lower wall.

Velocity profiles and friction factors for these surfaces are presented for ratios of air-injection velocity to mainstream velocity ranging from 0 to approximately 0.0170. For zero injection velocity the friction data compared favorably with available data on impermeable rough surfaces. It was found that the shape of the velocity profile is decidedly influenced by the fluid injection. The results also indicate in a qualitative manner the expected decrease in friction with increase in fluid injection.

INTRODUCTION

Transpiration cooling is receiving increased consideration as a means of reducing the temperature of walls exposed to hot gas streams to values the wall material can safely withstand. For such a cooling arrangement, the wall to be cooled is made of a porous material and a

coolant is blown through the pores and injected into the gas stream. In this way the air or coolant builds a cool film along the surface that protects the wall from the influence of the hot gases. The coolant also cools the wall by convection as it passes through the material. Applications for which this cooling method is considered are, for instance, the cooling of different structural elements like combustion chambers or turbine blades in jet engines, or the cooling of parts of the skin of missiles that are subjected to intensive aerodynamic heating.

A porous surface has by its nature a certain roughness that may influence to some degree the friction and heat transfer between the hot gas stream and the wall. Very limited information is available on the influence of surface roughness on heat transfer, even for solid surfaces. The result of a recent investigation is contained in reference 1 and summarized in reference 2. Some experimental studies of heat transfer for injections through a porous wall have been made (refs. 3 to 5) but without a systematic study of the influence of surface roughness. On the other hand, friction on rough solid surfaces has been investigated considerably in the past; and the information accumulated in a number of extensive investigations is summarized in several books (ref. 6, e.g.).

For this reason it was considered advantageous to obtain knowledge on friction of rough porous surfaces with fluid injection before the corresponding heat-transfer problem is attacked. Information on friction and especially on the velocity field near a porous wall was also considered useful. Such information would permit a check of assumptions utilized in the past to obtain theories on friction and heat transfer on a porous wall with fluid injection.

It may be reasoned that fluid injection may affect the friction of a rough porous surface in either of two opposite manners. It is known that fluid injection into an unbounded stream moving along a porous surface will increase the boundary-layer thickness. With this increase in boundary-layer thickness, however, the roughness elements of the porous wall may penetrate only into a reduced-velocity region. Such a state should lead to a smaller increase of friction due to surface roughness with fluid injection than on the same surface without injection. On the other hand, because of the finite pore size the coolant is actually injected from a porous surface in the form of jets. These jets may have enough energy to penetrate into the boundary layer a sufficient amount to cause turbulence. The turbulence, in turn, would tend to increase the friction and heat transfer. This latter process is mainly determined by the size of the pores and not by the surface roughness. In an actual porous material, however, both parameters are intimately connected.

Since nothing is known of these processes, an experimental investigation was initiated at the NACA Lewis laboratory in order to obtain information on the influence of surface roughness for porous walls on the development of the boundary layer and on the friction characteristics of the flow. This investigation was restricted to the conditions that the fluid injected through the porous surface and the fluid moving along the surface were both air and at the same temperature.

BASIC CONSIDERATIONS FOR FRICTION MEASUREMENTS ON ROUGH SURFACES

A basic difficulty in flow investigations on rough surfaces is connected with the fact that it is impossible to describe and classify a particular roughness to complete satisfaction. Such a description would have to include the shapes, sizes, and arrangement of the roughness elements. The previously mentioned investigations on the friction of rough surfaces show that the shape of the roughness elements has a considerable influence on the friction characteristics. The main parameter found in these investigations, however, was the ratio of the average height of the roughness elements to the thickness of the boundary layer; more specifically, to the thickness of that innermost portion of the boundary layer which is conventionally called the laminar sublayer.

In roughness investigations on boundary layers, the difficulty arises that in most cases (e.g., on a flat plate) the sublayer thickness changes locally along the surface in flow direction. The ratio of roughness height to sublayer thickness also changes locally even though the roughness height is constant along the surface. To circumvent this difficulty, the majority of investigations on rough surfaces have been made in tubes with fully developed flow. In this case, the laminar sublayer thickness is constant along the tube length and the investigation deals therefore with a constant ratio of roughness height to sublayer thickness. In addition, for developed flow, the velocities do not change in the direction of the flow.

On porous surfaces the advantage of an investigation in a tube is not fully realized when air is continuously injected through the porous tube walls, because the mass flow increases in downstream direction and therefore the velocity increases continuously. This increase in mean flow velocity is comparatively small, however, for injection rates of practical interest. As a consequence, the ratio of roughness height to sublayer thickness is expected to be practically constant over tube lengths necessary for friction measurements. Accordingly, the investigation of roughness effects in pipe flow seemed to promise advantages even for fluid injection as compared with an investigation in boundary-layer flow, provided fully established flow can be obtained with fluid injection. This provision, however, brings up the problem of how to create fully established flow.

As demonstrated in a calculation by Berman (ref. 7), a solution to the Navier-Stokes equations that is independent of the location in flow direction exists for laminar flow through a duct with fluid injection or suction through the porous walls at constant rate. In this solution, the shape of the velocity profile is independent of the location along the duct in the direction of flow - a criterion defining developed flow. It may be assumed that the actual flow through such a duct will finally adjust to this velocity distribution at sufficient distance from the inlet cross section. It may also be expected that the same behavior holds for turbulent flow. However, no information is available at present as to the length necessary to establish fully developed flow. It is necessary to perform roughness investigations in this flow region to ensure that the sublayer thickness is reasonably uniform over the tube length under investigation. There is still another advantage connected with the developed flow region which simplifies the determination of the friction coefficient and which will be discussed in the following paragraphs.

The friction which a fluid with constant density exerts in flowing through a passage can be obtained by measuring the static-pressure drop along the passage and the velocity profiles. When the pressure drop in a distance dx between two stations 1 and 2 (fig. 1) has been measured and when the velocity fields in both cross sections are known, the shearing stresses along the wall can be found from a momentum balance over the flow region limited by the tube walls and the two cross sections. If the cross-sectional area A is constant along x, the momentum balance yields

$$\int_C \tau_w \, dC = - A \frac{dp}{dx} - \frac{d}{dx} \int_A \rho u^2 \, dA \tag{1}$$

(All symbols are defined in the appendix.) In a passage with solid walls and under the condition of fully developed flow, the integral on the right side of this equation is independent of x, so that the last term becomes zero. If, in addition, the passage has a circular cross section, the shearing stress will be constant over the circumference of the tube, so that

$$\tau_w = - \frac{D}{4} \frac{dp}{dx}$$

With the definition of the friction factor in tube flow $- \frac{dp}{dx} = \frac{1}{D} f \rho \frac{\overline{u}^2}{2}$, the following equation results:

$$f = \frac{8 \tau_w}{\rho \overline{u}^2} \tag{2}$$

When a fluid is injected through the porous walls, the momentum integral over a flow cross section changes in flow direction, and the last term on the right side of equation (1) has to be retained. Quite often this term is of nearly the same magnitude as the pressure-drop term. Since the shearing stress is then obtained from the small difference of two terms of almost equal magnitude, an accurate experimental determination of the shearing stress with equation (1) is very difficult with injection at the wall. A simplification of this equation can be made when the flow in the passage with injection is developed. Such flow is defined by the condition that the ratio $u/\overline{u}$ is independent of x. By applying this similarity, equation (1) becomes

$$\int_C \tau_w \, dC = - A \frac{dp}{dx} - 2\overline{u}\left(\frac{d\overline{u}}{dx}\right)\int_A \rho\left(\frac{u}{\overline{u}}\right)^2 dA \tag{3}$$

According to this equation, the velocity fields must be measured in only one cross section, thus simplifying the determination of the friction coefficient.

Now

$$\overline{u}(x + dx) = \frac{1}{A}\int_r \int_C v_w(x,C) \, dC \, dx + \frac{1}{A}\int_A u(x) \, dA \tag{4}$$

The quantity $d\overline{u}/dx$ required in equation (3) is then obtained as

$$\frac{d\overline{u}}{dx} = \frac{1}{A}\int_C v_w \, dC$$

The following general rules are derived from the foregoing discussion. A cylindrical passage appears to offer advantages for an investigation of the roughness influence on flow and friction characteristics. Developed flow should be obtained in that portion of the passage in which the pressure-drop and velocity-profile measurements are made, and the passage cross section should be chosen so that the increase of the mean velocity in flow direction necessarily connected with fluid injection is kept small.

Not all these objectives are realized in the apparatus described in the next section. It was rather the intention of this preliminary investigation to collect information that will aid investigators in establishing the passage configuration that is most advantageous for such measurements and also to obtain some idea of the effects of surface roughness and injection at the wall on the velocity field and the friction.

APPARATUS

When this investigation was initiated, porous materials with different roughnesses were available only in a limited shape and length. All the general rules determined in the preceding section could not be incorporated in the design of the tunnel. Especially, the test section could not be made as large as appeared desirable for obtaining ideal flow conditions.

Test Channel

The tunnel (fig. 2) consists essentially of a rectangular channel 0.6 inch high and 3 inches wide. This height-to-width ratio was considered sufficient to make side wall effects small. Air is drawn from the test cell into this channel through a bellmouth, gauze filter, and straightening grid. The gauze and grid not only clean but straighten the flow and eliminate any disturbances entering from the test cell. The air enters the rectangular channel through a nozzle and flows at first through an impermeable approach section $23\frac{3}{8}$ inches long. This length was chosen to ensure that the flow enters the test section proper under fully developed conditions.

In the bottom wall of the test section a piece 6 inches long is made exchangeable. A solid plate as well as different porous materials can be provided in this portion. On the underside of this plate an air chamber is arranged through which air can be injected into the test section. The chamber is of sufficient size to assure good distribution of the air, which is admitted through two inlets. The condition of a locally uniform air-flow rate through the porous section into the interior of the channel can be further improved by proper choice of permeability of the bottom plate. The mainstream and injected air that leaves the test section is guided through a $6\frac{3}{8}$-inch section with the same rectangular cross section into a discharge chamber. This chamber finally is connected with the vacuum system of the laboratory. A similar arrangement has been used by Schlichting (ref. 8) for friction measurements on impermeable rough surfaces.

All solid surfaces in the present test channel were fabricated from steel 3/8 or 1/2 inch thick. The inside tunnel surfaces were ground smooth and the different portions of the channel carefully alined.

Surfaces Investigated

For the calibration of the tunnel, a smooth solid steel plate (1/4 by 3 by 6 in.) was provided in the exchangeable portion of the

bottom wall. The surface of the plate directed to the inside of the channel was ground to conform with the adjacent surfaces of the channel.

A bronze sintered plate (hereinafter designated as porous plate) of the same size was used as one of the porous surfaces for the lower wall. Measurements of the surface irregularities indicated an arithmetical average roughness of 0.0045 inch. The largest observed roughness height was 0.0055 inch, and the smallest, 0.0032 inch. From an enlarged photo of the surface of the porous plate, the average size of the pores was found to be 0.008 inch and the average distance between the pores, 0.006 inch. For a preliminary check, the porous plate was installed in the test section, the top cover of the test section was removed, and air flow was directed through the porous plate by pressurizing the air chamber below the test-section bottom wall. The uniformity of the flow through the porous plate was found to vary irregularly over the entire plate surface by ±10 percent from the average value. Other porous materials produced by sintering that have been checked at this laboratory for flow uniformity showed deviations of at least the same magnitude. This nonuniformity of the flow turned out to be one of the main difficulties in the investigations described in this report.

Surfaces with increasing roughness were formed by placing stainless steel wire screens on top of the porous plate. The screens used in the following investigations are of mesh sizes 20×350 with 0.008-inch-diameter wire, 20×120 with 0.010-inch-diameter wire, and 7×26 with 0.018-inch-diameter wire. These diameters are for one of the many wires indicated as vertical wires in the plan views of figure 3. The wire screens were oriented in the test section with the greater number of wires perpendicular to the main flow direction. The screens were carefully located at the bottom section of the tunnel in such a way that the highest points of their surfaces were in line with the solid walls upstream and downstream of the test section.

Air-Flow System

Room air at about 80° F was drawn through the channel by the laboratory altitude exhaust system to which the downstream end of the tunnel was connected. The exhaust system operates from atmospheric pressure to 20 inches of mercury below atmospheric. The air flow through the tunnel was regulated with valves downstream of the test section. A rotameter was included in the air-flow path to obtain a direct measurement of the air-flow rate.

The air injected into the tunnel through the porous plate was dry air pressurized up to 10 pounds per square inch gage with temperature of about 80° F. Dry air was used because of its cleaner quality. A throttle valve in the system regulated the air-flow rate, which was measured with a rotameter.

MEASUREMENTS AND INSTRUMENTATION

Pressure

A schematic diagram of the instrumentation of the tunnel is shown in figure 4(a). Total-pressure traverses were obtained at three stations in the test section and one station downstream. The first (front) station was located in the cross section in which the porous wall started and in the central location along the width of the tunnel. Other stations were arranged at $2\frac{1}{2}$ inches (midstation) and at 5 inches (rear station) downstream of the front station in the center plane of the tunnel width.

Total-pressure surveys were obtained for some tests in a cross section 1 inch downstream of the test section and along the three verticals indicated in figure 4(a). The purpose of these readings was mainly to indicate the uniformity of the flow along the tunnel width; they also gave interesting information on the development of the flow after it left the porous wall.

The total-pressure surveys were made with a probe shown in figure 4(b). The probe was fabricated from 0.050-inch-outside-diameter tubing with 0.007-inch wall thickness. The tip of the tube was flattened to an oval shape with a vertical height of 0.030 inch and the large axis of the oval arranged parallel to the bottom and top walls of the channel. With these probes, total-pressure readings were obtained from about 0.030 inch from the bottom wall to within approximately 0.050 inch of the top wall. The probe was moved by a motor-driven mechanism. An electric circuit was interrupted as soon as the probe touched the upper or lower wall; in this way the zero position of the probe could be fixed.

Static-pressure measurements were observed in the same planes in which the total-pressure measurements were taken. The static pressures were obtained by tapping the upper wall with a 0.020-inch-diameter drill. Any burrs caused by the drilling of the taps were very carefully eliminated. At least three taps were used at each station to obtain an average reading across the upper tunnel wall, and it was assumed that the static pressure was constant over the tunnel height in each cross section.

All pressures in the test section were measured on micromanometers with water as fluid. Other pressures not in the test section below 2 pounds per square inch gage were observed on a water manometer board; pressures above 2 pounds per square inch gage were measured on a mercury manometer board.

Temperatures and Weight Flows

Bare-wire iron-constantan thermocouples were used to measure air temperatures in the inlet and discharge chambers as well as the temperature of the air injected into the tunnel through the porous surfaces. Air-flow rates were obtained directly from rotameter readings. These rotameters were calibrated under operating conditions. A check on these measurements was possible from the total-pressure surveys and the static-pressure measurements.

Accuracy of Measurements

The accuracy of the total- and static-pressure readings observed on the micromanometers is believed to be within 0.04 inch of water. Approximately half this variation can be attributed to reading accuracy and the other half to fluctuations. The location of the center of the total-pressure probes within the tunnel could be determined within about 0.002 inch. The upper wall of the tunnel was used as the reference point for the probe positioning. All manometer-board pressure measurements are within 0.05 inch of water or mercury. Temperature measurements are accurate within 2° F. Calibrations of the rotameters indicated an accuracy of 1 percent.

EXPERIMENTAL PROCEDURES

The flow approaching the test section is fully developed. If the main flow is suddenly subjected to the injection of air and in this way deformed within the test section itself, the flow is again in an undeveloped state. Therefore, equation (1) has to be used for a calculation of the friction coefficients. Assuming a unit width and assuming that the flow is two-dimensional in the center plane of the channel in which the total-pressure traverses are taken, and considering that the pressure drop is measured along a finite length Δx, equation (1) transforms into

$$\tau_{w,s} + \tau_{w,r} = - h \frac{\Delta p}{\Delta x} - \frac{1}{\Delta x}\left[\left(\int_0^h \rho u^2 \, dy\right)_2 - \left(\int_0^h \rho u^2 \, dy\right)_1\right] \qquad (5)$$

The shearing stresses on the upper and lower channel walls can be expressed by friction factors according to equation (2). These friction factors will be symbolized by f_s and f_r, indicating that the upper tunnel wall was always a smooth solid surface, whereas the lower tunnel wall was the exchangeable porous rough surface. Thus, equation (5) becomes

$$f_s + f_r = -\frac{8h\Delta p}{\rho \bar{u}_{av}^2 \Delta x} - \frac{8}{\bar{u}_{av}^2 \Delta x}\left[\left(\int_0^h u^2\,dy\right)_2 - \left(\int_0^h u^2\,dy\right)_1\right] \qquad (6)$$

where the friction factors are based on an average velocity defined by

$$\bar{u}_{av}^2 = \frac{\bar{u}_1^2 + \bar{u}_2^2}{2}$$

An evaluation of the friction factor f_r from equation (6) requires a measurement of the static-pressure drop Δp and of the velocity profiles in the two cross sections separated by Δx. In addition, the friction coefficient f_s of the upper smooth surface has to be known. The determination of this friction coefficient will now be discussed.

The initial runs in the tunnel were made with a solid smooth plate installed in the lower channel wall of the test section. The purpose of these runs was to calibrate the tunnel and to determine the friction factor f_s. These runs were made after checks for air leakage through the tunnel joints were obtained by comparison of weight-flow readings based on the rotameter and on the velocity-profile surveys. Agreement of the air-flow rate between the probe survey and the rotameter was within 2 percent. It is believed that the deviation in flow resulted from instrument inaccuracy rather than from leakage. It should be noted that for the runs with the smooth solid plate the integrals in equation (6) are identical and can be omitted.

The next series of runs was made on the porous plate. The ratio of injection velocity through the porous plate to the main flow velocity was varied from zero to about 0.017. The injected air velocity is based on the total area of the porous plate. The mainstream velocity is based on the inlet area of the test section. The Reynolds number Re for the tests with air injection was held to a value of about 6.0×10^4. This Reynolds number was determined by the capacity of the piping system. The arrangement of the instrumentation did not permit simultaneous surveys at the middle with the front and rear stations. Therefore, the individual runs were repeated for observations at the front and middle stations. This procedure was repeated for the 20×350, 20×120, and 7×26 wire mesh screens.

EXPERIMENTAL VELOCITY DISTRIBUTIONS

In order to determine the two-dimensionality of the flow in the center plane of the tunnel, velocity surveys were taken for a number of runs in a cross section 1 inch downstream of the test section. The

location of the verticals along which these surveys were taken is indicated in figure 4(a). As an example of these velocity surveys, figure 5 presents the results of one run for the porous plate. The front and rear profiles are included for comparison. The three profiles are nearly identical, especially near the lower wall. The maximum deviation in the average velocity $\overline{u}$ of the three downstream profiles is approximately 2 percent. The differences in the other runs were of the same order of magnitude. This particular run presents the condition where nonuniformity in flow would be most apparent, since the porous plate indicated noticeable variations in permeability. High injection airflow rates as shown here would also make flow irregularities more apparent.

It should be noted at this point that the locations of the total-pressure readings were corrected to account for the displacement of the reading due to pressure gradients. This correction was applied as indicated in reference 9, which states that the displacement of the reading from the probe center line towards the high-pressure side is 0.18 of the outside probe diameter. In this investigation, the probe diameter was taken as 0.030 inch, thus giving a displacement of about 0.005 inch.

Figure 6 shows the velocity profile obtained at the front and rear stations in the first runs in which the lower wall of the test section consisted of a smooth solid surface. The profiles measured at the front and rear stations are practically identical. A slight asymmetry of the profile is also discernible. This asymmetry was found in all the following experiments, and no reason for it could be determined.

Figure 7 presents the velocity profiles measured by the front, mid, and rear probes for the test series in which the porous plate was used as the lower wall of the tunnel. Increasing air flows (figs. 7(a) to (f)) were injected through this plate into the tunnel. It is interesting to observe how the velocity profile in the mid and rear station gradually deforms as compared with the front profile in a degree increasing with increasing injection air flow. The deformation of the velocity profile on a boundary layer along a porous wall was similarly observed in reference 10. Both observations prove definitely that the influence of the fluid injection reaches deep into the main flow and that the assumption on which available theories have been based (viz., the influence of the injection is restricted to the thin laminar sublayers) does not correspond to reality. It may also be observed that the midstation profile is different from the rear-station profile. This difference indicates that developed flow has not formed in about the first half of the test-section length. Additional surveys between the mid and rear stations would be necessary to determine whether developed flow resulted downstream of the midstation. A more detailed comparison and evaluation of the profiles of figure 7 is made subsequently.

Figure 8 presents the front and rear velocity profiles obtained with screens of different roughness for the condition of no flow through the wall. This figure can be compared with figure 6 and shows how a velocity profile is deformed when fully developed flow is suddenly subjected to a rough surface. It can be clearly recognized that increased deformation of the profile occurs for increased roughness of the surface. The influence of a rough surface on the velocity profile appears to be similar to the influence of fluid injection for low injection rates. The large scale of figure 8 permits drawing of separate curves for the front and rear profiles for figure 8(a). This was not apparent in figure 7(a) because of the reduced scale.

Early investigations by Nikuradse established the fact that velocity profiles in fully developed flow of channels with rough or smooth surfaces are represented on a semilogarithmic plot by approximately straight lines (ref. 11). Thus, deviations of the velocity profiles measured in this investigation from the established profile on solid surfaces can be more clearly distinguished in a semilogarithmic plot than in the presentation used up to now. For this reason, the velocity profiles on the porous plate are once more presented in figure 9(a) with the inclusion of the profiles measured in the middle station. Figures 9(b) to (d) show similar profiles for the different wire screens.

The following observations can be made on the presented velocity profiles. The profiles are never exactly straight lines; even for zero injection flow rates the linearity predicted by Nikuradse's universal log law is not apparent. Similar nonlinearity is also discernible upon careful study of the data of Schlichting (ref. 8) and has also been found to occur over Nikuradse's original data (ref. 12). For large injection rates the profiles on the semilogarithmic plots become quite concave, indicating that actually fluid injection transforms the velocity profiles in a way different from a rough surface. Probably the velocity component normal to the surface at the porous wall causes, by displacement, velocity components in the same direction even in air layers quite far away from the surface. These layers are moved into a range of larger velocities in the main flow direction, and the corresponding momentum increase is compensated by a change in the profile shape. A theory of turbulent flow with fluid injection has to account for this phenomenon if the actual conditions are to be described.

A comparison of the different profiles measured on surfaces with different roughnesses for no flow through the porous wall with the profiles for the maximum flow rates is also interesting. Such a comparison is given in figure 10. The roughness of the surface has a decidedly larger influence for no flow than for injection flow. This trend might indicate a condition that with increasing flow rates the roughness of the surface has a decreasing influence on the flow process and correspondingly also on the friction characteristics of the surfaces.

A comparison of the velocity profiles measured in the upper portion of the channel bounded by the upper channel wall was made in the same way as for the lower half. On these profiles, with flow as well as for no flow, lines with a slight concave curvature were obtained on a semilogarithmic plot. Only one example of such profiles is shown (fig. 11). Examination of the data shown in figure 11 for zero injection flow indicates that the velocity at the rear station is somewhat larger than at the other stations for the same distance from the wall. This same effect is also shown on the left side of figure 8(a) for the front and rear stations. This velocity increase in flow direction results from the development of the flow over the rough surface. From the fact that these profiles all correspond in shape to the universal law established by Nikuradse, it is concluded that the upper half of the velocity profile feels the effect of what happens to the lower half only insofar as the velocity maximum may be displaced from the center plane of the tunnel and as the absolute amount of the velocities may be increased by a displacement of the flow. However, the shapes of the profiles, and consequently the law describing the friction on the upper surface, are not changed. This constancy in the friction law for the upper wall justifies the use of the friction coefficient as it was determined in the channel with the smooth solid wall installed as the lower wall. Schlichting also found that the smooth-wall friction is not affected by the rough wall (ref. 8). This assumption is used for the evaluation of equation (6) when a rough surface is arranged on the lower tunnel wall and when fluid is injected into the tunnel.

EVALUATIONS AND COMPARISONS WITH PREVIOUS INFORMATION

Velocity Distributions

The following general laws for velocity profiles in fully developed tube flow have been established by measurements of Nikuradse. The relation for the velocity distribution in a pipe with smooth solid walls is (ref. 6, p. 369):

$$\frac{u}{u^*} = 5.75 \log \frac{yu^*}{\nu} + 5.5 \tag{7}$$

A recent analysis of Nikuradse's data in reference 12 indicates that the use of a value of 5.6 for both the constant and the coefficient is more applicable. In the present investigation, however, this change has little significance. Therefore, equation (7) will be used. For a pipe with a rough or a smooth surface, the difference between the maximum velocity in the center of the pipe and the local velocity u still follows a universal relation given by the following equation (ref. 11, or ref. 6, p. 372):

$$\frac{u_m - u}{u^*} = 5.75 \log \frac{r}{y} \tag{8}$$

where, for symmetrical profiles in the present experiments, $r = h/2$; for unsymmetrical profiles r expresses the distance of the velocity maximum from the channel wall.

Figure 12 shows the upper-wall velocity profiles divided by u^*, calculated from tunnel data, for zero injection flow with smooth or rough surfaces as the lower wall of the tunnel. These data are compared with the general relation (universal velocity distribution) in a pipe with smooth walls (eq. (7)). In general, good agreement is obtained, the average deviation being about 6 percent. The measured velocities are generally lower than the line indicating the universal velocity profile, because the tunnel walls could not be considered as completely smooth hydraulically. This is also indicated by the fact that the friction factors, which will be presented later for the "smooth" tunnel, are somewhat above the previously established friction factors for a pipe with smooth surfaces. When u/u^* is calculated with equation (7), in which u^* is obtained from the tunnel data, better agreement is indicated, as shown by the dashed line in figure 12. Since the results shown in figure 12 indicate the tunnel not to be completely smooth hydraulically, a comparison using equation (8) for smooth and/or rough surfaces was also made. Figure 13(a) gives $(u_m - u)/u^*$ against the ratio of the distance of the velocity maximum from the upper wall to distance of the local velocity from the wall and also the general universal velocity distribution law (eq. (8)). The larger values of $(u_m - u)/u^*$ for the data compared with the universal relation for a given r/y may be attributed to the fact that the flow in the tunnel was slightly asymmetric. This asymmetry, already noted in the discussion of figure 6, results in a lower value of u near the upper wall and, therefore, a larger value of $(u_m - u)/u^*$. It is expected that asymmetry becomes more apparent when results are presented on the basis of $(u_m - u)/u^*$ (fig. 13), whereas lack of hydraulic smoothness is better indicated by u/u^* (fig. 12).

The same check on the relation of the velocity defect (eq. (8)) was made with the velocities measured on the lower portion of the profile and with the different rough surfaces for no flow condition. Figure 13(b) presents this comparison with the general law (eq. (8)) and indicates good agreement. No attempt was made to correlate the data for air injection, since a relation was not available. Use of equation (8) for the correlation of these data would require the exact determination of the friction coefficient from which u^* is calculated. For this investigation the results of the friction coefficients are only of a qualitative nature.

Friction Coefficients

No air injection. - Friction factors for the no-flow condition were calculated with equation (6). The evaluation procedure for the smooth

plate in the lower wall is straightforward. The result is indicated by the lowest test points in figure 14. This series of points is somewhat higher than those obtained from the relation of Blasius (ref. 6, p. 363). The agreement, however, is considered reasonable. For the evaluation of the four rough surfaces, it was assumed that the value f_s obtained from the already mentioned test series applies also for the upper wall. Figure 14 indicates a continuous increase of the friction factor with the increase in roughness parameter.

A comparison will now be made of the friction factors in figure 14 with previously published data. In this connection, it has to be kept in mind that the present measurements apply strictly to the condition where flow, which has become fully developed in a channel with smooth walls, is subjected to the changed boundary condition implied by a rough surface and adjusts itself to this condition. It has to be expected that friction factors for this condition will be somewhat higher than values for fully developed flow in a channel with rough surfaces.

Measurements are reported in reference 1 for flow through circular tubes with regular roughnesses which were generated by milling rectangular grooves in the inside surface of the tubes. The friction coefficients for two values of the roughness parameter k/r are inserted as dashed lines in figure 14. These friction factors are approximately in the range that agrees with the friction factors measured for corresponding roughness parameters in this report. Very close agreement cannot be expected because of the difference in the character of the roughness reported in reference 1. In addition, for the investigation reported herein the flow was apparently not fully developed.

The effect of the roughness height on the friction factor is shown more clearly in figure 15, where the abscissa is the relative roughness k/r. The top curve is for the quadratic law of resistance

$$f = (1.74 + 2 \log r/k)^{-2} \qquad (9)$$

as determined by Nikuradse in his experiments with sand as roughness elements (ref. 11). In the region wherein equation (9) is applicable, the friction factor is independent of the Reynolds number. The lower curve in the figure was obtained by cross-plotting Nikuradse's results (fig. 9 of ref. 11) at $Re = 6 \times 10^4$.

Sand was also used as one of the roughnesses in the investigation by Schlichting (ref. 8). It is expected that the data of Nikuradse and Schlichting should be in good agreement, since the roughness element was the same. It may be noted in figure 15 that this is the case when the friction factor measured by Schlichting is plotted over the relative roughness based on half the tunnel height r rather than on the

hydraulic radius r_h. The ratio k/r_h had been used by Schlichting as roughness parameter. The heights of the other roughnesses investigated by Schlichting were larger than the roughness height of the sand and are not given in figure 15.

The results of the present experiments, read from figure 14, are given in figure 15 on the basis of r and are in reasonable agreement with Nikuradse's results. This agreement indicates that the roughness elements of the samples tested are similar to sand roughness. The data of reference 1 determined for square-thread roughness are also given in the figure. It has already been pointed out in reference 1 that the roughness ratio k/r is not an adequate measure of relative roughness for square-thread passages. This inadequacy may be noted by comparison of the f value given by the higher curve and the data point from reference 1 at $k/r = 0.016$ for the square-thread roughness.

The proximity of a roughness sample to sand roughness may also be determined by building the ratio k_σ/k where k_σ is the equivalent sand roughness and k is the actual roughness height. By equivalent sand roughness k_σ is meant that grain size of sand roughness which has, according to equation (9), the same resistance as the given roughness k. Thus, from the friction data and curves in figure 15, the equivalent sand roughness k_σ and the dimensionless ratio k_σ/k can be determined for the various roughnesses. The results are given in table I for the present data as well as for the data of Sams and Schlichting (refs. 1 and 8). In reference 8 the hydraulic radius was used in the determination of k_σ; the values of k_σ given in table I are based on the half tunnel height r. These values of k_σ are smaller, therefore, than the values given in reference 8, since $r/r_h = 0.617$ for the test section of that reference. The values of k_σ/k for the results of reference 8 are arranged in increasing relative roughness for each type of roughness element. In most cases, larger k_σ/k is the result of larger roughness density (i.e., more roughness elements per unit surface area). Only for three of the samples investigated by Schlichting is the ratio k_σ/k close to 1. These roughnesses are Hamburg sand IX, the hemisphere XIX, and the short angle XVIII, as may be noted in table I. As noted in the discussion of figure 15, the data of the present report are in fair agreement with the data of Nikuradse. This agreement is also indicated in table I by the fact that for the present roughnesses $k_\sigma/k \approx 1$.

Air injection. - Friction factors were also calculated for the different porous surfaces under condition of fluid injection with the help of equation (6). The results of the calculation are presented in figure 16. The porous sintered plate results are not shown, since the

calculated friction factor dropped below zero even for values of $v_w/\overline{u} = 0.004$. This negative friction factor is obviously impossible. The surface with the largest roughness (7×26 mesh screen) also shows a variation of the friction factor that deviates considerably from the character of the friction factor for the other two screens. An examination of the test data revealed that the flow rates measured by the rotameter did not agree well with the flow rates measured by the pressure probes for the porous plate as well as for the largest roughness sample. This lack of agreement is probably connected with the fact that the flow was not sufficiently uniform locally on both these surfaces, as mentioned in the APPARATUS section. For large flow rates the correction caused by the last term in equation (6) becomes very large, so that slight deviation from the correct flow rate influences the friction factor markedly. Generally, the precision with which the determination of friction factors could be made for flow through the porous surfaces should not be overestimated, and figure 16 should be used only to show the general trend of the friction factor.

An attempt was made to check the influence of an error in the flow measurements on the friction factor. For this purpose it was assumed that the momentum change in the main flow depends only on velocity ratio $v_w/\overline{u}$ but not on the surface roughness. The measurements on the 20×120 screen were used to obtain this momentum change for the other roughness samples also; the result of this calculation procedure is shown in figure 17. For the porous plate, this procedure again resulted in negative friction factors for flow rates larger than 0.004. Comparison of figures 17 and 16 shows that the difference in friction factors for the various roughnesses is reduced at larger injection flow rates.

CONCLUSIONS

From an experimental investigation on porous rough surfaces, the following conclusions are obtained:

1. The shape of the velocity profile is decidedly influenced by a fluid injection from the surface. Theories on turbulent friction and heat transfer with fluid injection should account for this variation of the profile in order to describe real conditions adequately.

2. The specific way in which the velocity profile is influenced by fluid injection differs from the influence by surface roughness. This difference is indicated by the fact that in a semilogarithmic plot the profile with fluid injection becomes decidedly nonlinear.

3. The velocity profile in the neighborhood of a solid wall opposite to a rough or porous wall is influenced only insofar as the

velocity maximum is displaced. In addition, the magnitude of the velocities may be increased by the flow displacement. However, the character of the flow, and accordingly the law describing the velocities and the friction, is not changed.

4. Friction factors for a porous sintered surface and for three wire screens with different roughnesses without air injection indicate that the increase in friction due to the surface roughness is nearly the same as that found by Nikuradse for surfaces with sand roughness. This similarity applies if the ratio of roughness height to half tunnel height is the same in both cases.

5. Evaluations of the friction factors for the porous surfaces with fluid injection show qualitatively a decrease in friction. The accuracy of these evaluations was not sufficient to determine quantitatively the friction factors under the condition of fluid injection. Velocity profiles indicate that the influence of roughness parameter decreases with increasing injection velocity.

6. With injection through the porous wall, the flow was not fully developed in about half the length of the test section where velocity profiles were observed. The ratio of the tunnel length where the velocity profiles were observed to the height for this arrangement was 5.

Lewis Flight Propulsion Laboratory
National Advisory Committee for Aeronautics
Cleveland, Ohio, October 29, 1954

APPENDIX - SYMBOLS

The following symbols are used in this report:

A	cross-sectional area
C	circumference
D	diameter
F	projected surface area
F_r	projected area of roughness elements
f	friction coefficient
h	tunnel height
k	roughness height
p	pressure
Re	Reynolds number, $2\bar{u}r_h/\nu$
r	pipe radius or distance from wall to maximum velocity
r_h	hydraulic radius, 2A/C
s	pitch of roughness elements
u	velocity parallel to wall
u^*	shearing-stress velocity, $\bar{u}\sqrt{f/8}$
v	velocity normal to wall
x	distance parallel to wall
y	distance normal to wall
μ	absolute viscosity of fluid
ν	kinematic viscosity of fluid, μ/ρ
ρ	density of fluid
τ	shear stress

Subscripts:

av	values averaged over length
m	maximum
r	rough
s	smooth
w	wall
σ	sand
1,2	station locations

Superscript:

$\bar{}$	values averaged over a cross section

REFERENCES

1. Sams, Eldon W.: Experimental Investigation of Average Heat-Transfer and Friction Coefficients for Air Flowing in Circular Tubes Having Square-Thread-Type Roughness. NACA RM E52D17, 1952.

2. Pinkel, Benjamin: A Summary of NACA Research on Heat Transfer and Friction for Air Flowing through Tube with Large Temperature Difference. Trans. A.S.M.E., vol. 76, no. 2, Feb. 1954, pp. 305-318.

3. Weinbaum, Sidney, and Wheeler, H. L., Jr.: Heat Transfer in Sweat-Cooled Porous Metals. Jour. Appl. Phys., vol. 20, no. 1, Jan. 1949, pp. 113-122.

4. Canright, Richard B.: Preliminary Experiments of Gaseous Transpiration Cooling of Rocket Motors. Prog. Rep. No. 1-75, Power Plant Lab., Proj. No. MX801, Jet Prop. Lab., C.I.T., Nov. 24, 1948. (AMC Contract No. W-535-ac-20260, Ord. Dept. Contract No. W-04-200-ORD-455.)

5. Friedman, Joseph: A Theoretical and Experimental Investigation of Rocket-Motor Sweat Cooling. Jour. Am. Rocket Soc., no. 79, Dec. 1949, pp. 147-154.

6. Schlichting, Herman: Grenzchicht-Theorie. G. Braun, Karlsruhe, 1951.

7. Berman, Abraham S.: Laminar Flow in Channels with Porous Walls. Jour. Appl. Phys., vol. 24, no. 9, Sept. 1953, pp. 1232-1235.

8. Schlichting, H.: Experimental Investigation of the Problem of Surface Roughness. NACA TM 823, 1937. (See also condensed version, ref. 6; pp. 385-386.)

9. Young, A. D., and Maas, J. N.: The Behaviour of a Pitot Tube in a Transverse Total-Pressure Gradient. R. & M. No. 1770, British A.R.C., Sept. 9, 1936.

10. Mickley, H. S., Ross, R. C., Squyers, A. L., and Stewart, W. E.: Heat, Mass, and Momentum Transfer for Flow over a Flat Plate with Blowing or Suction. NACA TN 3208, 1954.

11. Nikuradse, J.: Strömungsgesetze in rauhen Rohren. VDI-Forsch. 361, Bd. 4, July/Aug. 1933. (Also available in English translation as NACA TM 1292.)

12. Ross, Donald: A New Analysis of Nikuradse's Experiments on Turbulent Flow in Smooth Pipes. Proc. Third Midwestern Conf. on Fluid Mech., Univ. of Minnesota, Mar. 23-25, 1953, pp. 651-667.

TABLE I. - EQUIVALENT SAND ROUGHNESSES

Roughness sample	r, in.	s, in.	k, in.	F_r/F	k_σ, in.	k_σ/k	
Porous plate							
Re = 6×10^4	0.3	-----	0.0045	-------	0.00438	0.973	
Eq. (9)	↓	-----	------	-------	.00324	.720	
Wire screen							
20×350 mesh	0.3	Tightly packed	0.008	-------	0.00844	1.06	
20×120 mesh	↓	Tightly packed	.010	-------	.01224	1.22	
7×26 mesh	↓	0.038	.018	0.594	.0218	1.21	
Square threads* (ref. 1)							w, in.
A	0.25	0.0094	0.0065	0.500	0.01018	1.566	0.0047
B	↓	.0195	..0095	.564	.0070	.737	.0085
C	↓	.0094	.0042	.500	.0023	.578	.0047
Hamburg sand (ref. 8)							
IX	0.787	------	0.0532	-------	0.0539	1.01	
Spheres** (ref. 8)							
XII	0.787	1.575	0.161	0.00785	0.0226	0.140	
V	↓	Tightly packed	↓	.907	.0624	.388	
III	↓	.787	↓	.0314	.0836	.519	
I	↓	.394	↓	.126	.306	1.90	
II	↓	.236	↓	.349	.379	2.35	
VI	↓	.394	.0827	.0314	.0418	.505	
IV	↓	.197	.0827	.126	.184	2.22	
Hemispheres** (ref. 8)							
XIII	0.787	1.575	0.1024	0.0087	0.0075	0.0732	
XIV	↓	1.181	↓	.0155	.0119	.117	
XV	↓	.787	↓	.0348	.0362	.354	
XIX	↓	Tightly packed	↓	.251	.0887	.868	
Cones** (ref. 8)							
XXIII	0.787	1.575	0.1476	0.0106	0.0143	0.0969	
XXIV	↓	1.181	↓	.0189	.0399	.270	
XXV	↓	.787	↓	.0425	.0909	.616	
Short angles† (ref. 8)							t, in.
XVI	0.787	1.575	0.1181	0.0151	0.0707	0.599	0.315
XVIII	↓	1.181	↓	.0269	.150	1.27	↓
XVII	↓	.787	↓	.0605	.357	3.02	↓
Long angles‡ (ref. 8)							
XX	0.787	2.36	0.1260	0.0538	0.440	3.49	[a]6.69"
XXI	↓	1.575	.1220	.0776	.899	7.37	↓
XXII	↓	.787	.1181	.152	.865	7.32	↓

[a] Tunnel width.

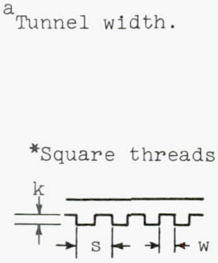

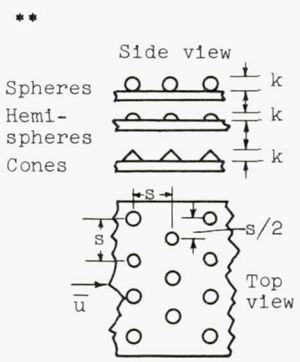

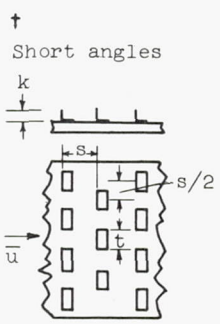

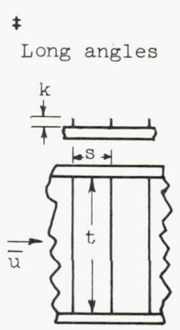

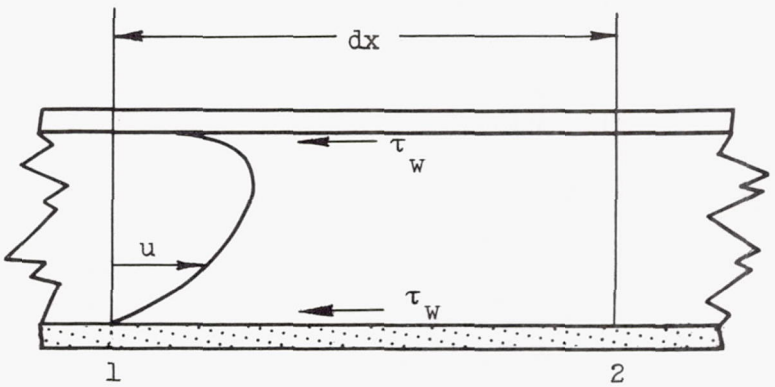

Figure 1. - Velocity and shear stress in channel.

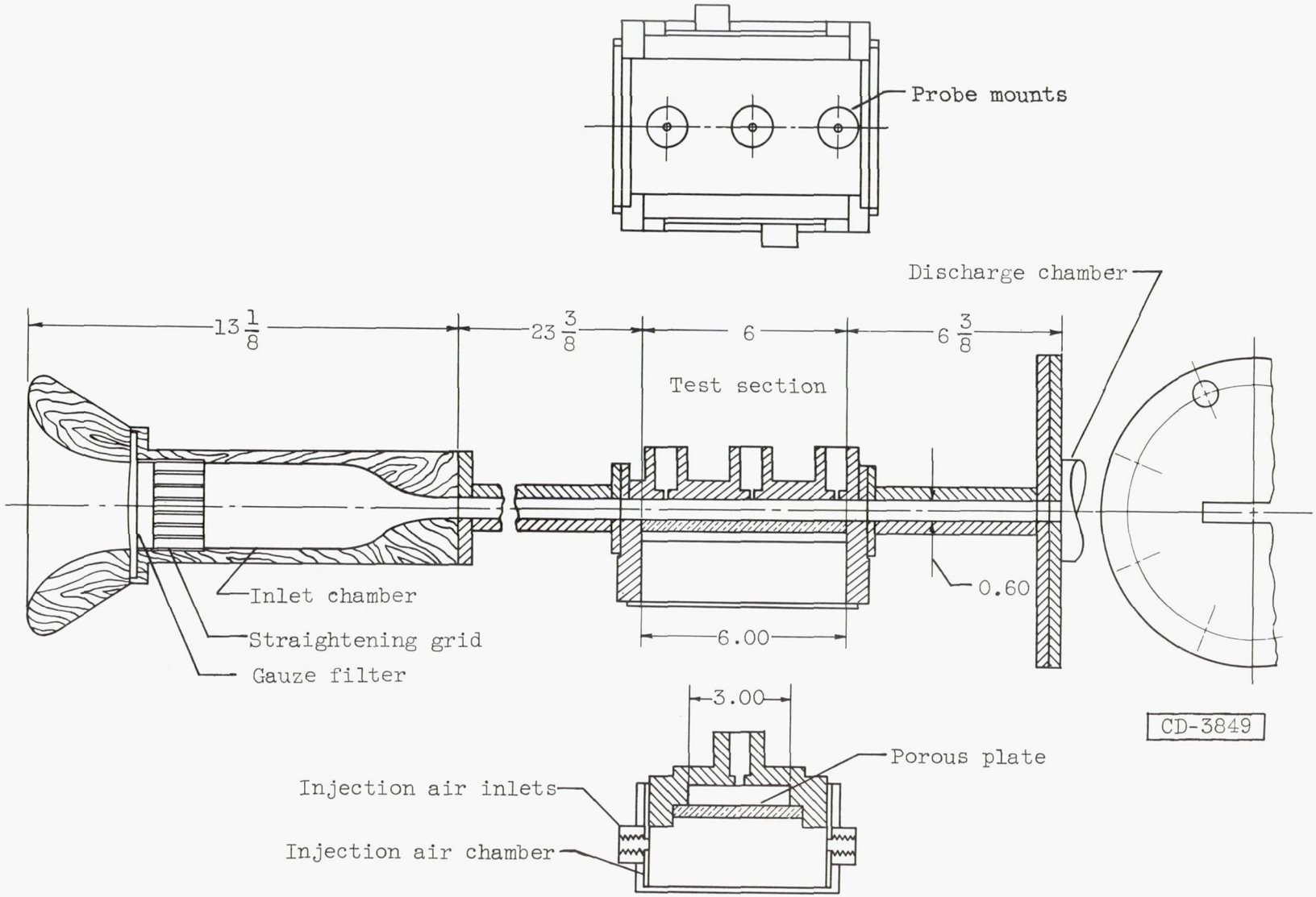

Figure 2.- Cross section of tunnel. (All dimensions in inches.)

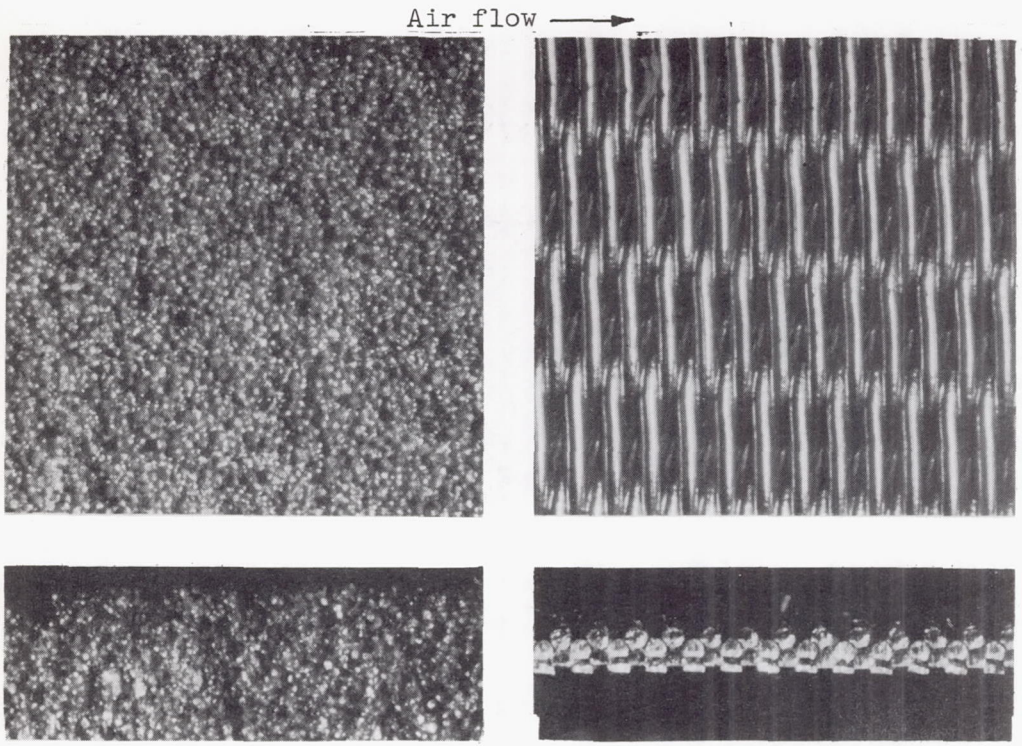

(a) Porous plate.

(b) Wire screen, 20×350 mesh.

(c) Wire screen, 20×120 mesh.

(d) Wire screen, 7×26 Mesh.

Figure 3. - Roughness samples (magnified).

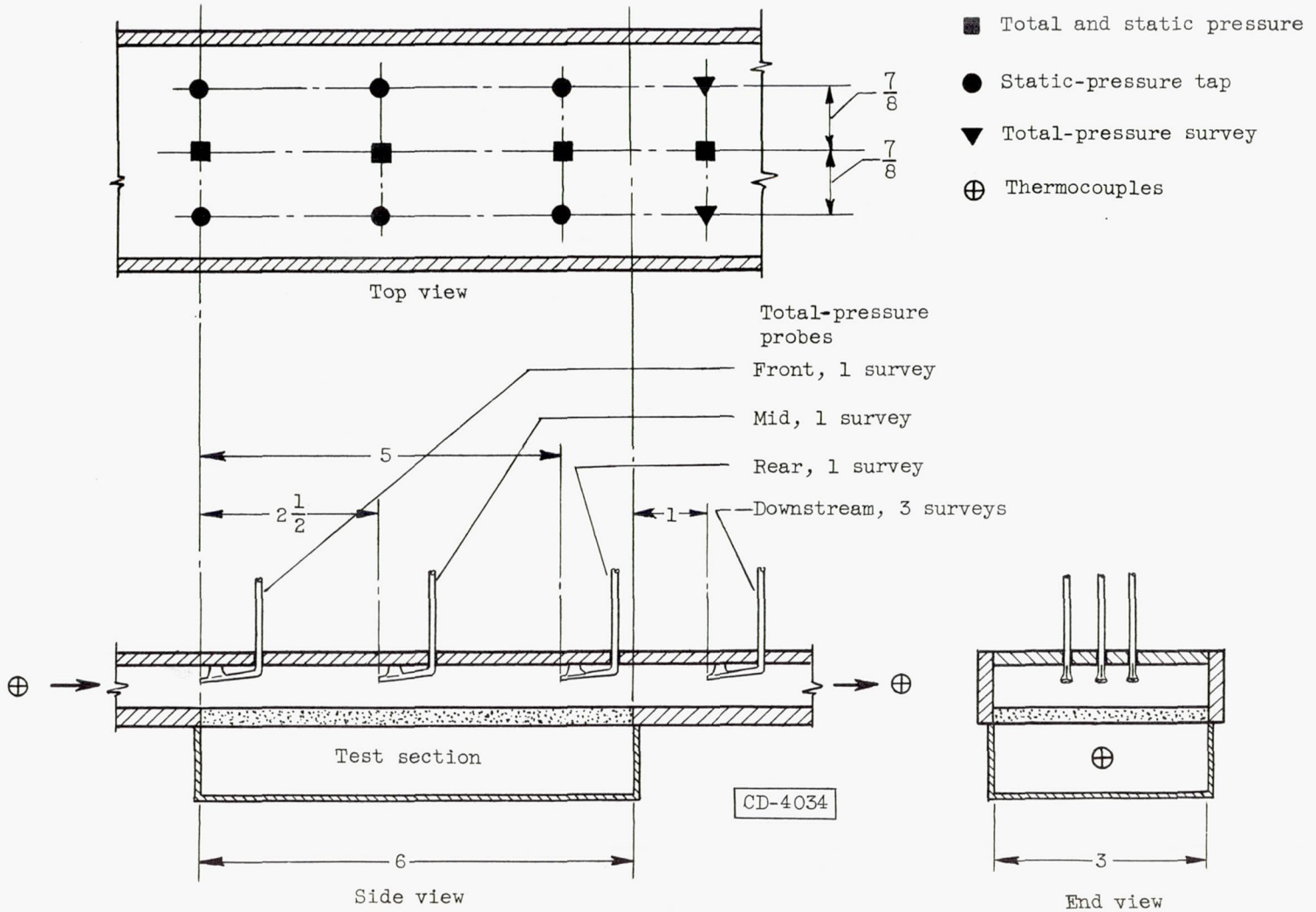

(a) Tunnel test section.

Figure 4. Instrumentation. (All dimensions in inches.)

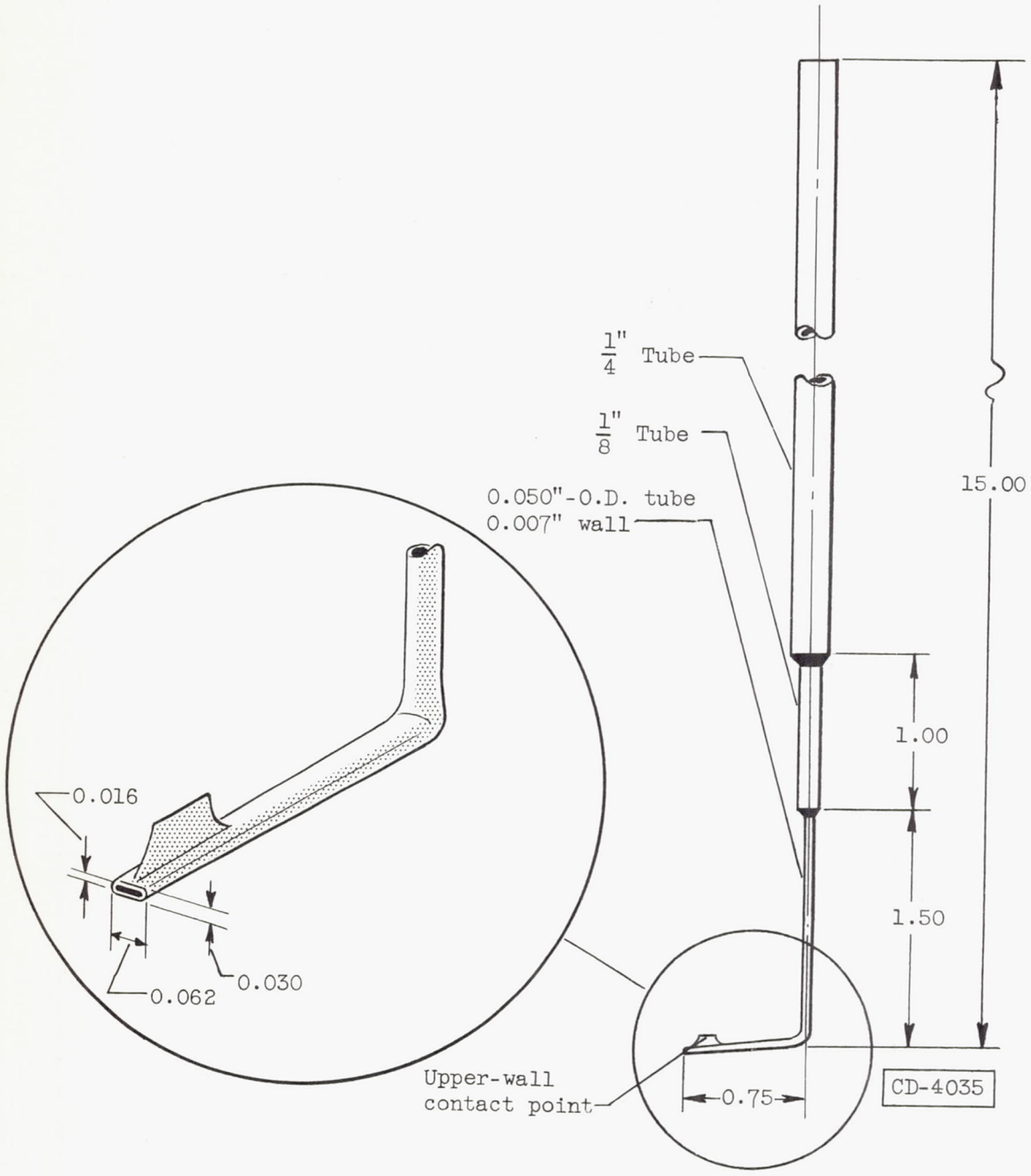

(b) Total-pressure probe.

Figure 4. - Concluded. Instrumentation. (All dimensions in inches.)

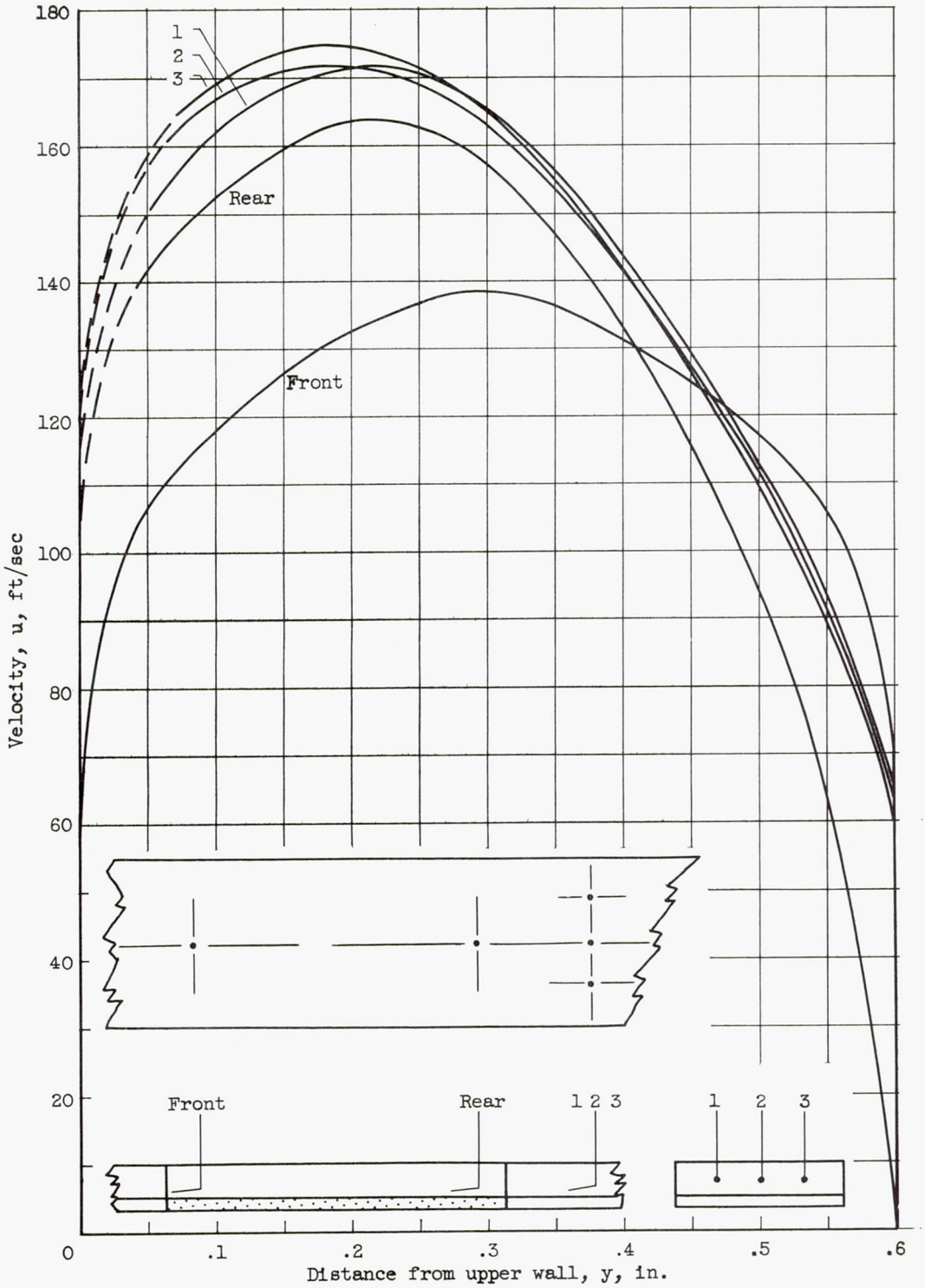

Figure 5. - Velocity profiles across channel with porous-plate lower wall for front, rear, and downstream stations. Reynolds number, 6×10^4; velocity ratio, $v_w/\bar{u}_1$, 0.0172.

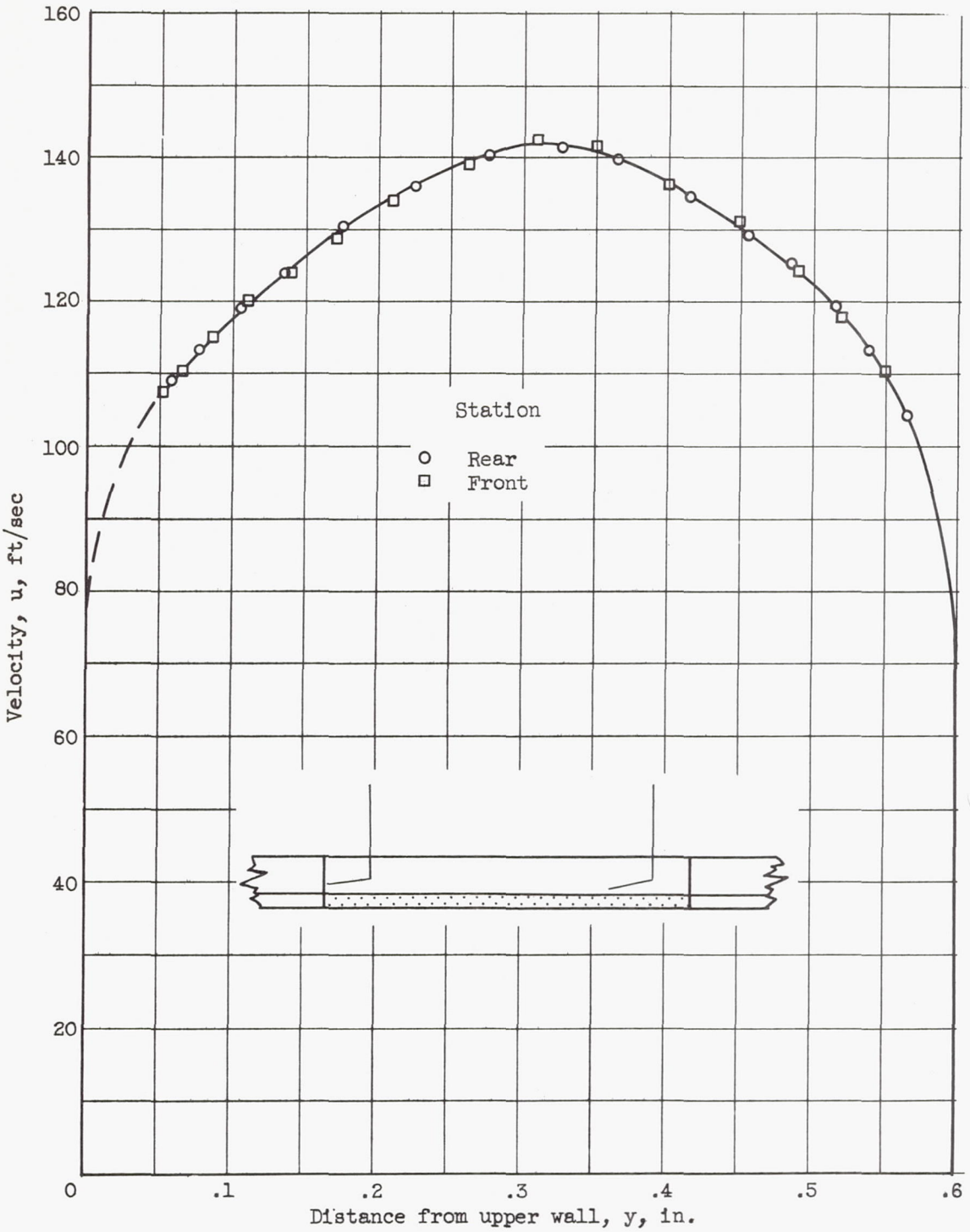

Figure 6. - Velocity profiles across channel for front and rear stations with smooth solid-plate lower wall. Reynolds number, 6×10^4.

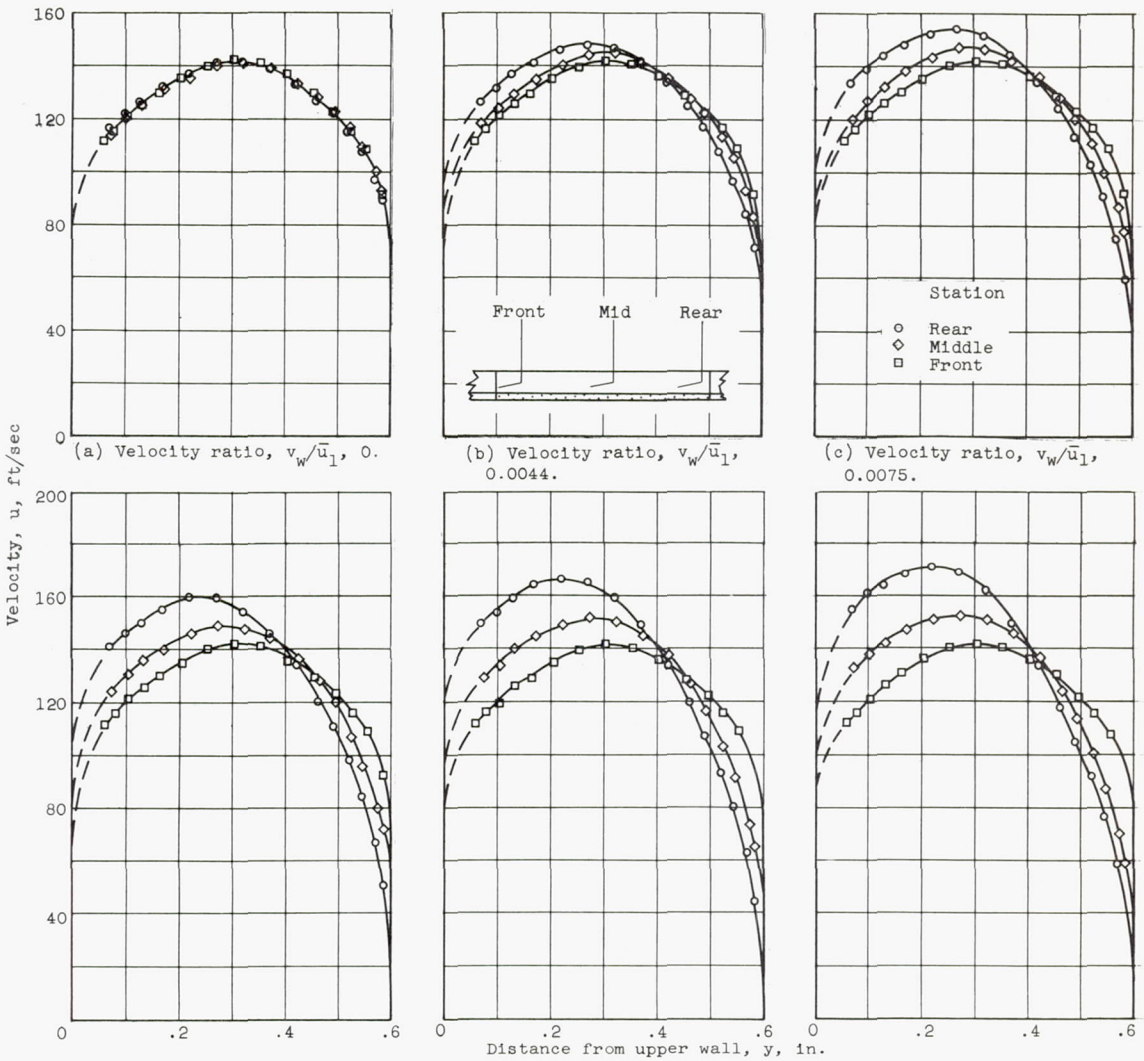

(a) Velocity ratio, $v_w/\bar{u}_1$, 0.

(b) Velocity ratio, $v_w/\bar{u}_1$, 0.0044.

(c) Velocity ratio, $v_w/\bar{u}_1$, 0.0075.

(d) Velocity ratio, $v_w/\bar{u}_1$, 0.0107.

(e) Velocity ratio, $v_w/\bar{u}_1$, 0.0144.

(f) Velocity ratio, $v_w/\bar{u}_1$, 0.0168.

Figure 7. - Velocity profiles across channel for porous-plate lower wall at front, middle, and rear stations with air injection.

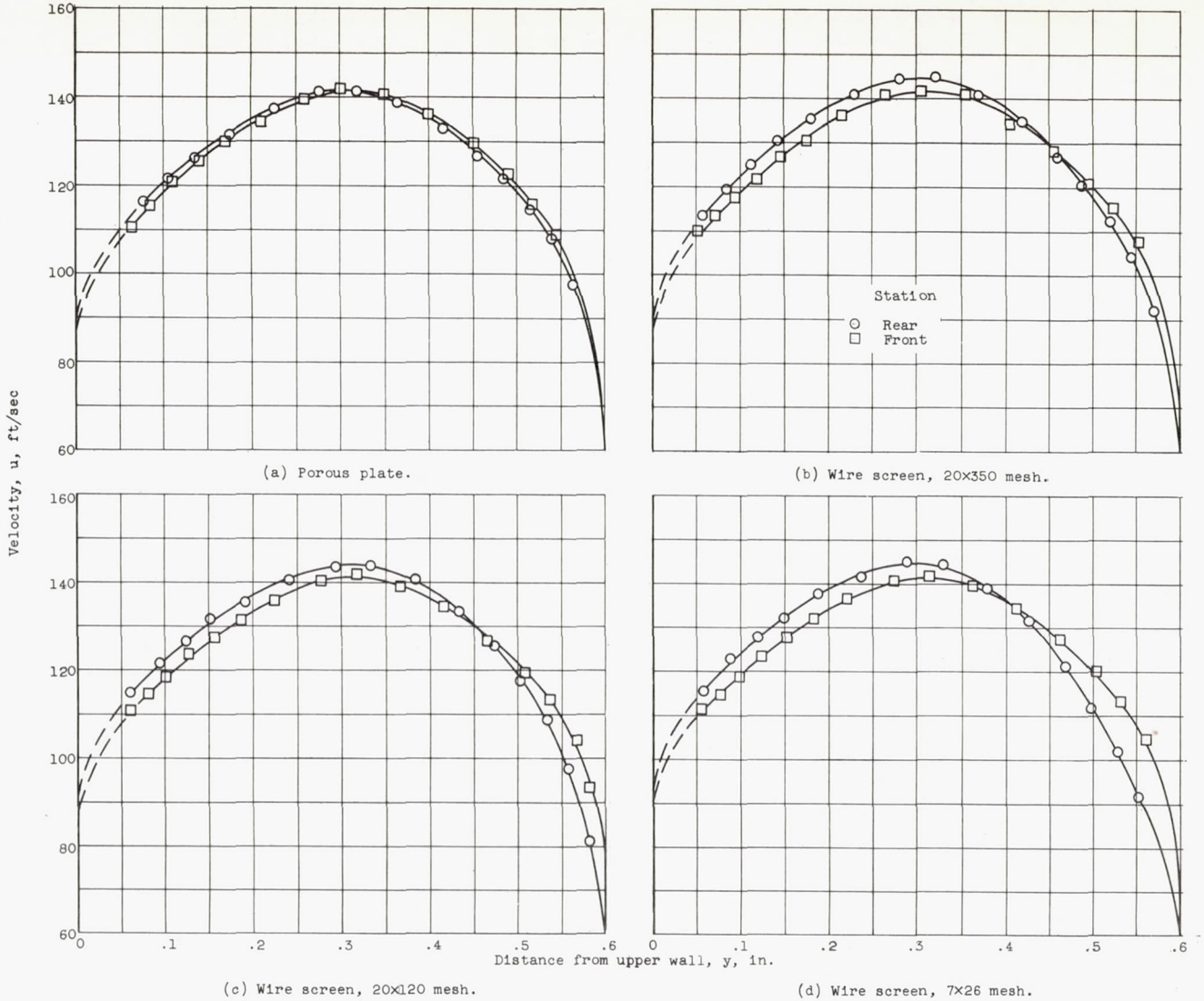

(a) Porous plate.

(b) Wire screen, 20x350 mesh.

(c) Wire screen, 20x120 mesh.

(d) Wire screen, 7x26 mesh.

Figure 8. - Velocity profiles across tunnel at front and rear stations with rough-surface lower wall. Velocity ratio, $v_w/\bar{u}_1$, 0.

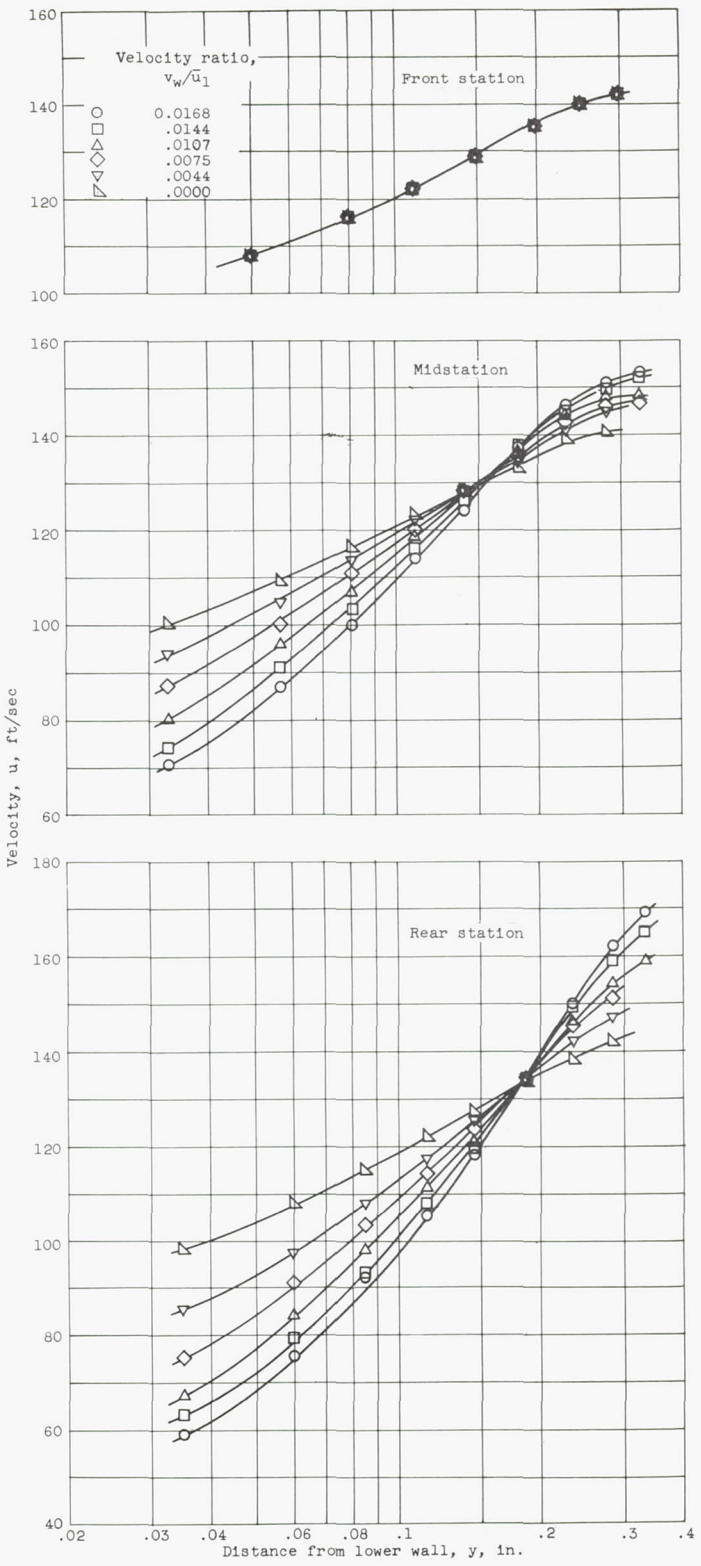

(a) Porous plate.

Figure 9. - Velocity profiles near lower wall.

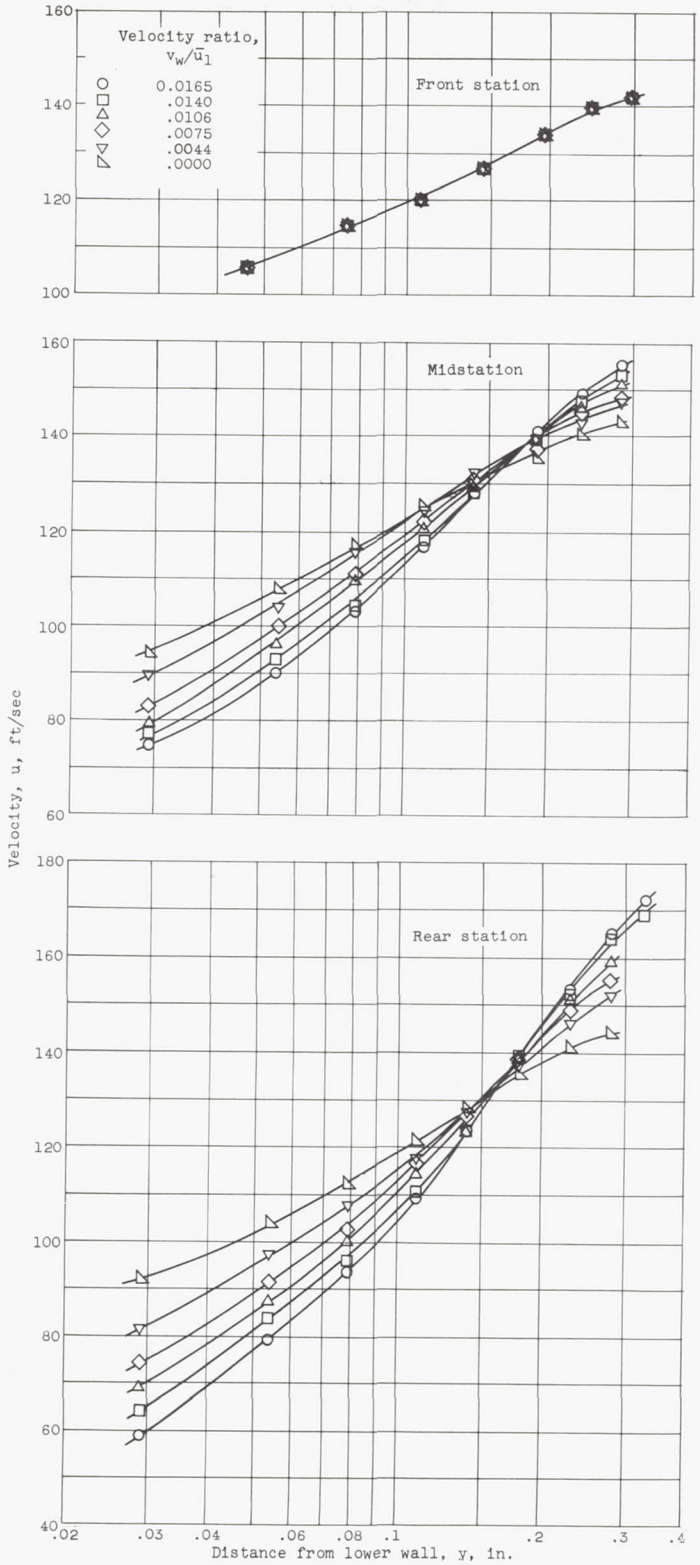

(b) Wire screen, 20×350 mesh.

Figure 9. - Continued. Velocity profiles near lower wall.

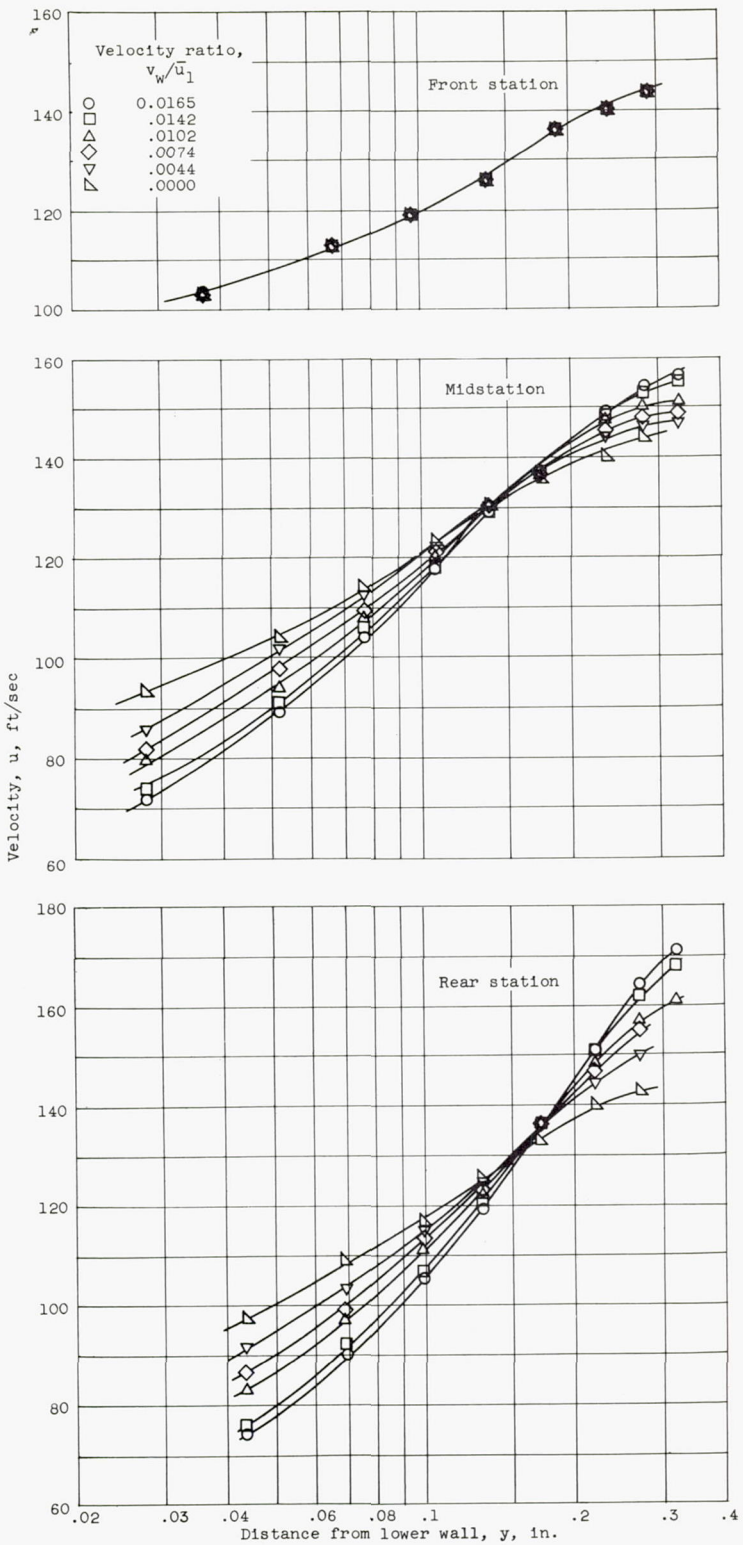

(c) Wire screen, 20×120 mesh.

Figure 9. - Continued. Velocity profiles near lower wall.

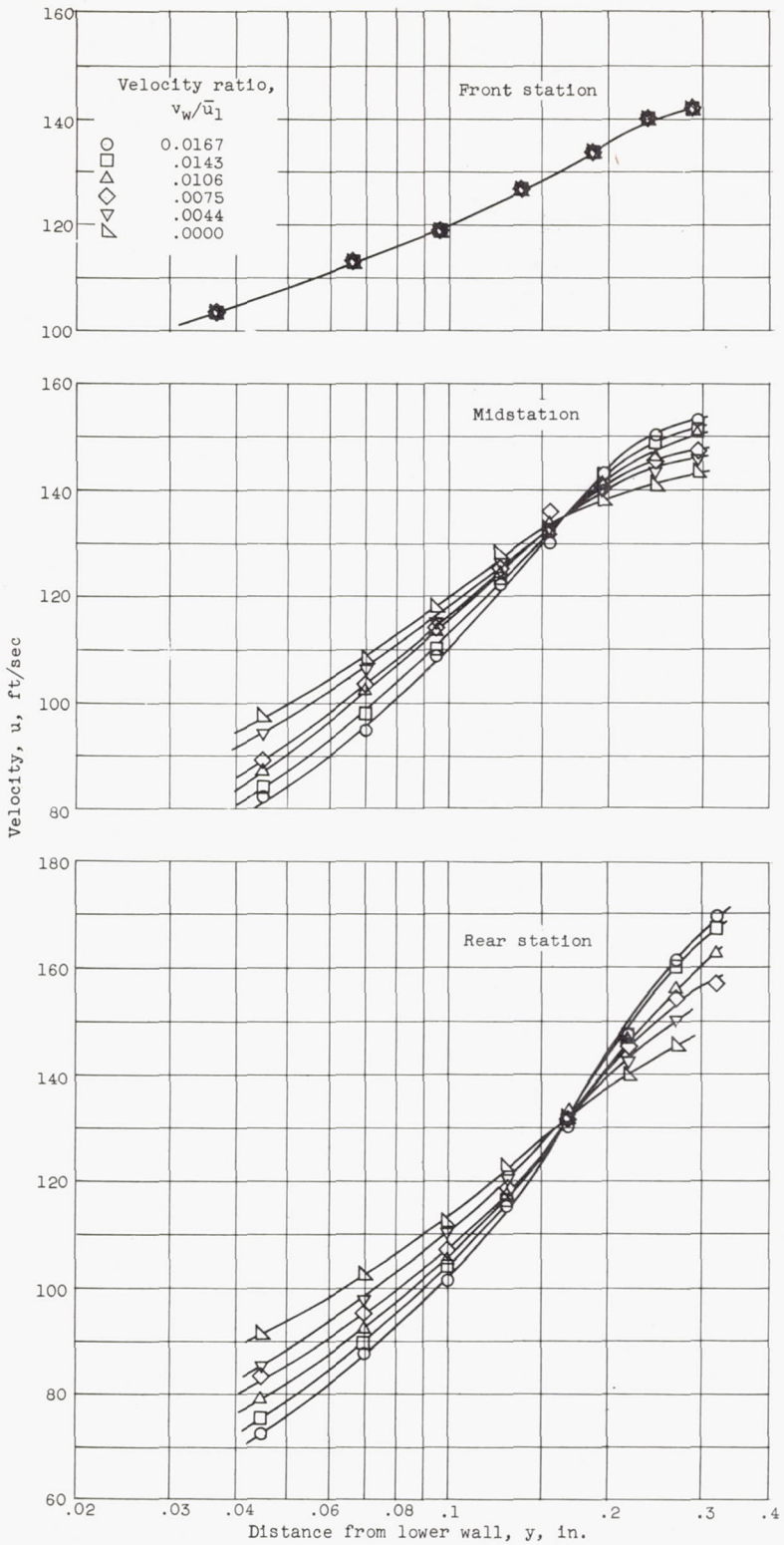

(d) Wire screen, 7x26 mesh.

Figure 9. - Concluded. Velocity profiles near lower wall.

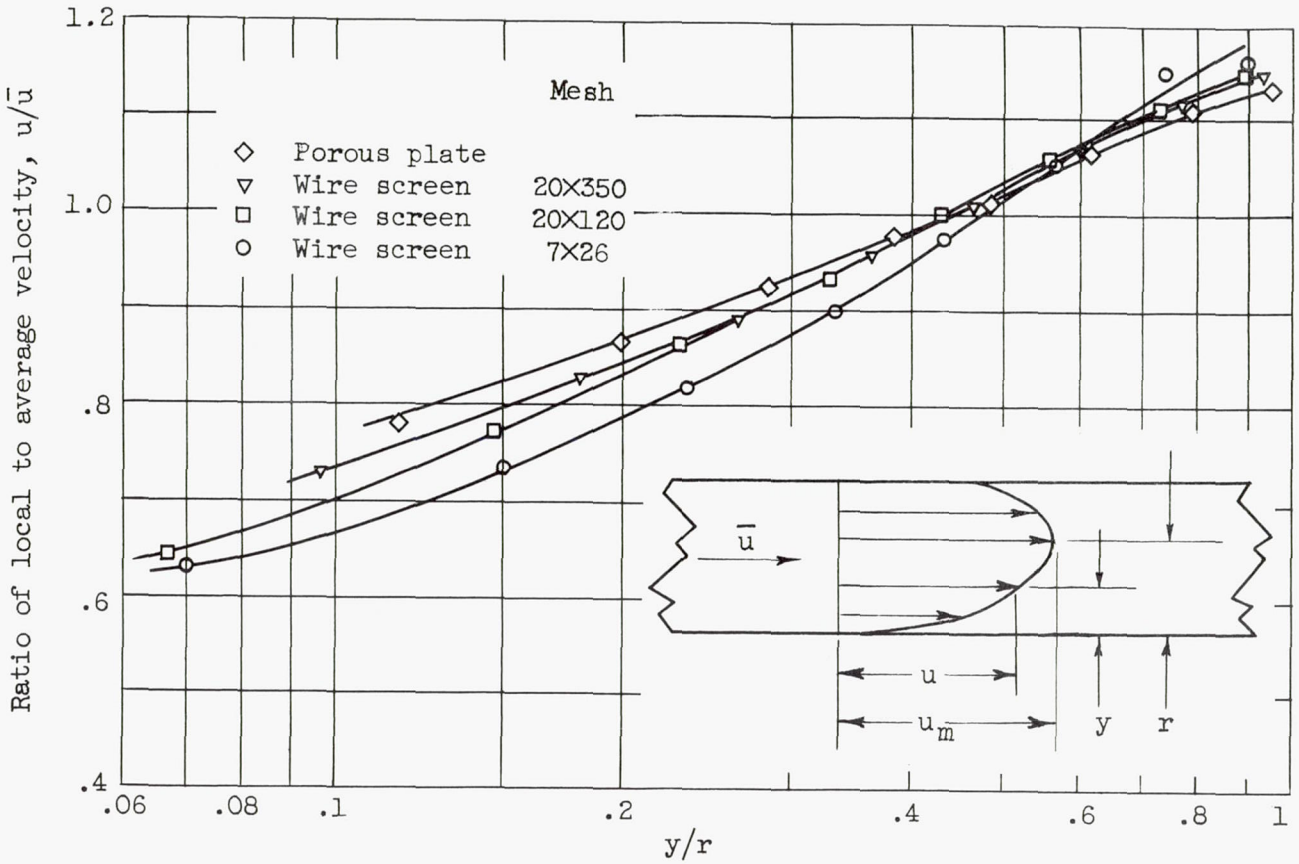

(a) Velocity ratio, $v_w/\bar{u}_1$, 0.

Figure 10. - Profiles of ratio of local to average velocities near lower wall for varying roughness of lower wall. Rear station.

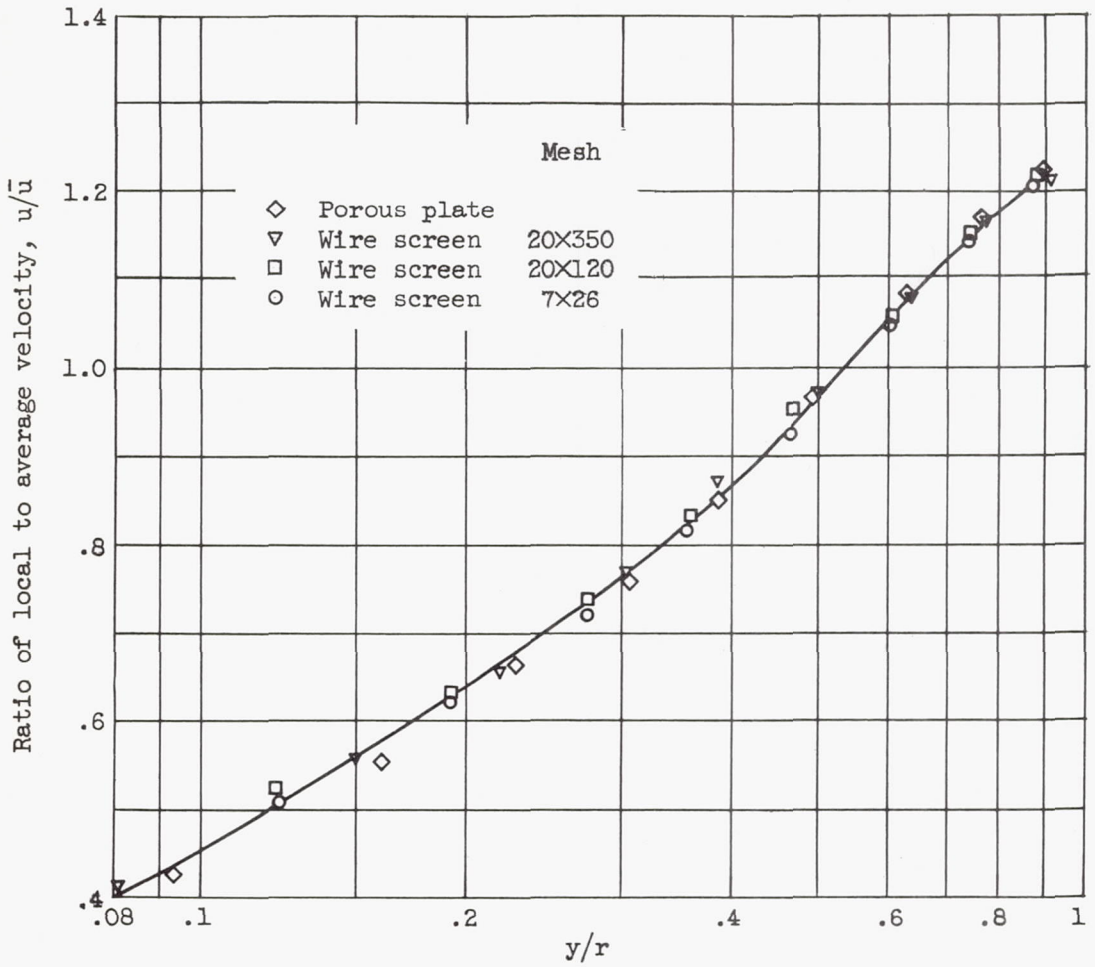

(b) Velocity ratio, $v_w/\bar{u}_1$, 0.0165.

Figure 10. - Concluded. Profiles of ratio of local to average velocities near lower wall for varying roughness of lower wall. Rear station.

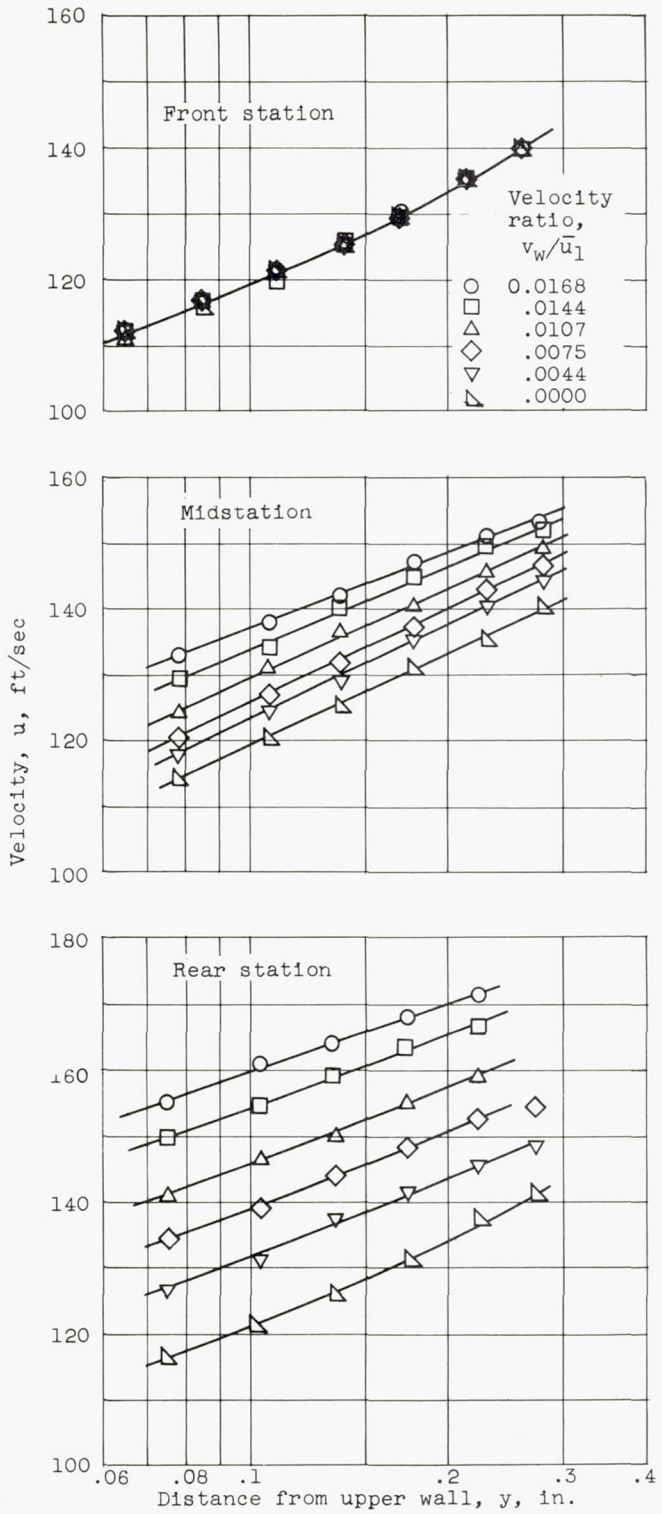

Figure 11. - Velocity profiles near smooth upper wall with porous-plate lower wall.

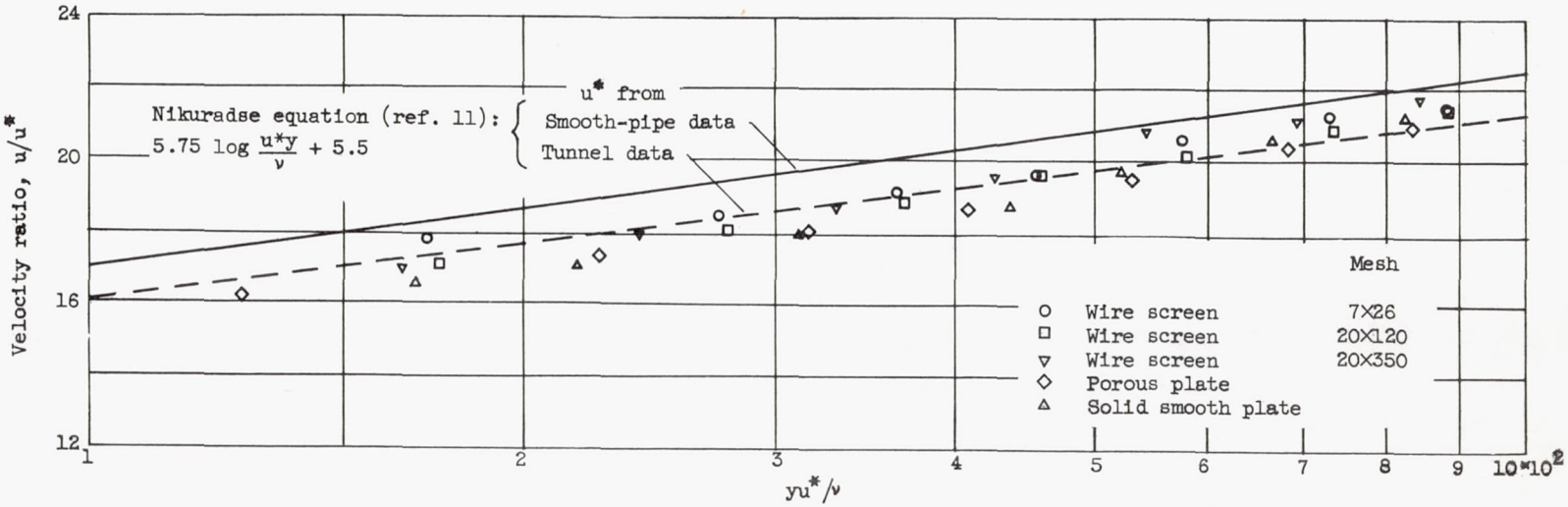

Figure 12. - Comparison of tunnel data for upper wall with universal velocity distribution law for smooth pipes. Rear station; no air injection.

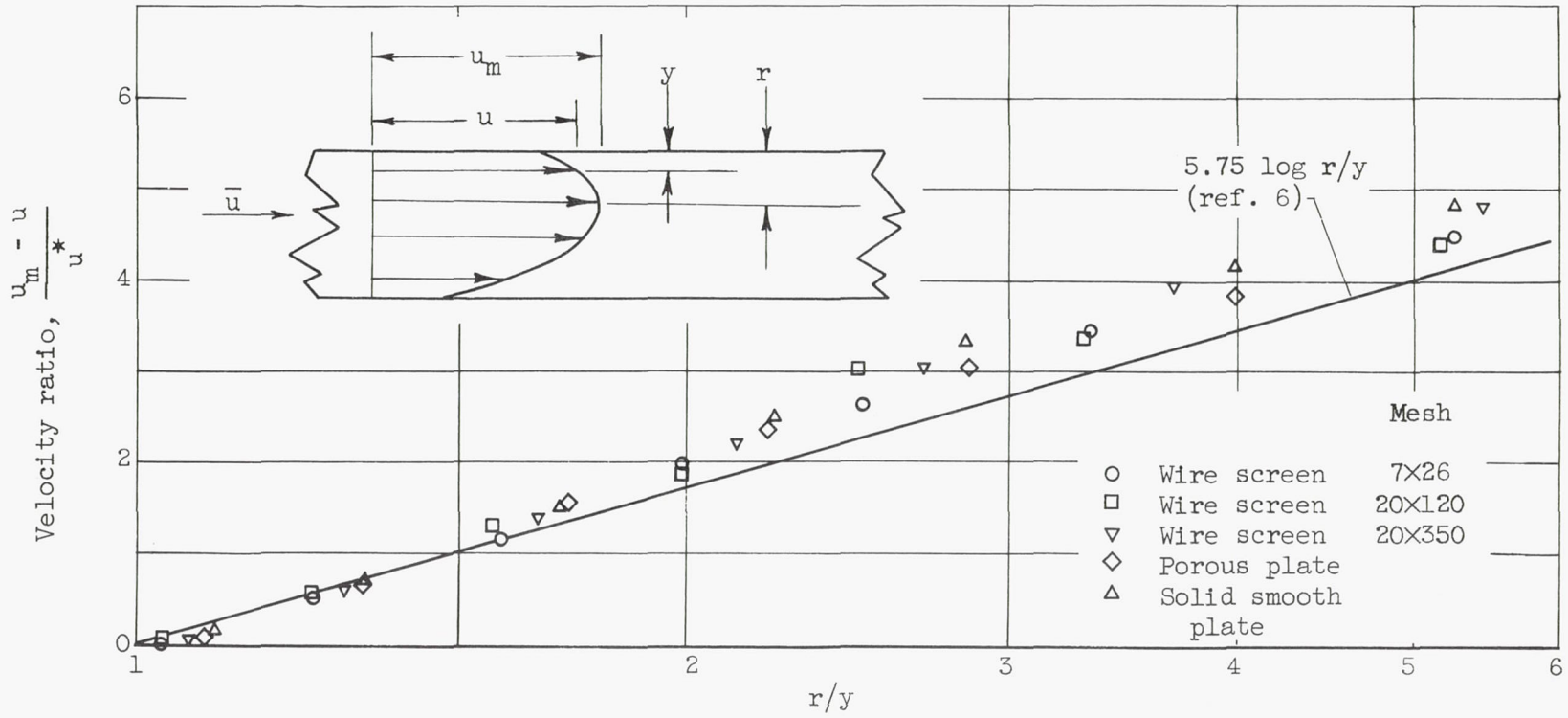

(a) Near upper wall.

Figure 13. - Velocity-profile correlation for upper or lower wall with varying roughness of lower wall. Rear station; no air injection.

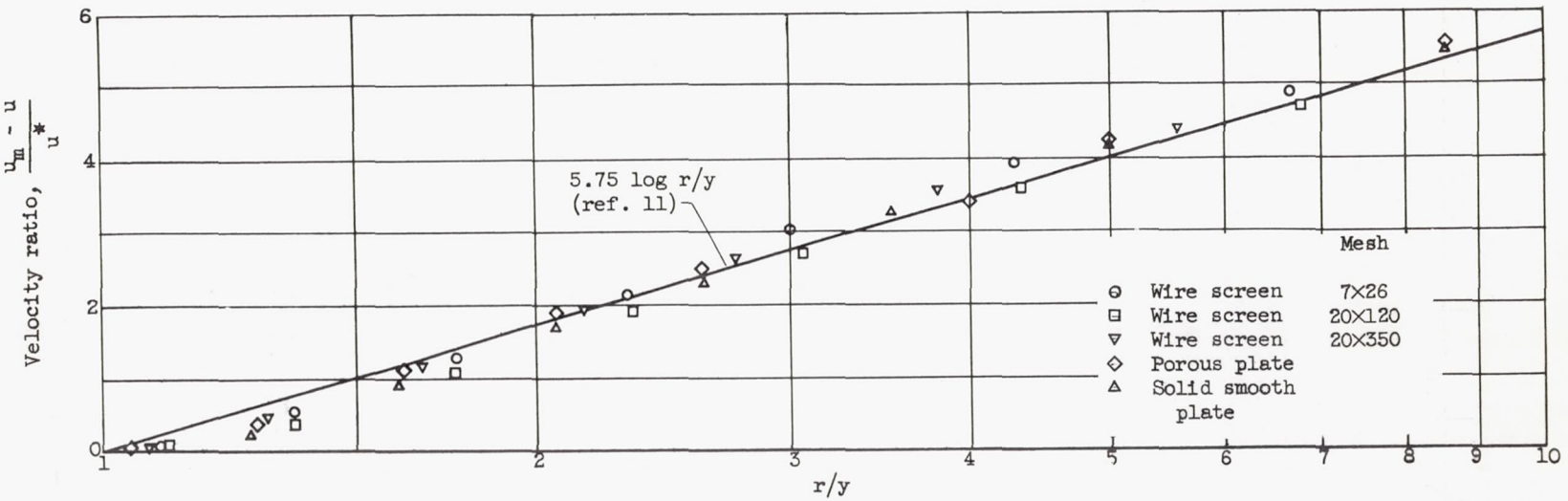

(b) Near lower wall.

Figure 13. - Concluded. Velocity-profile correlation for upper or lower wall with varying roughness of lower wall. Rear station; no air injection.

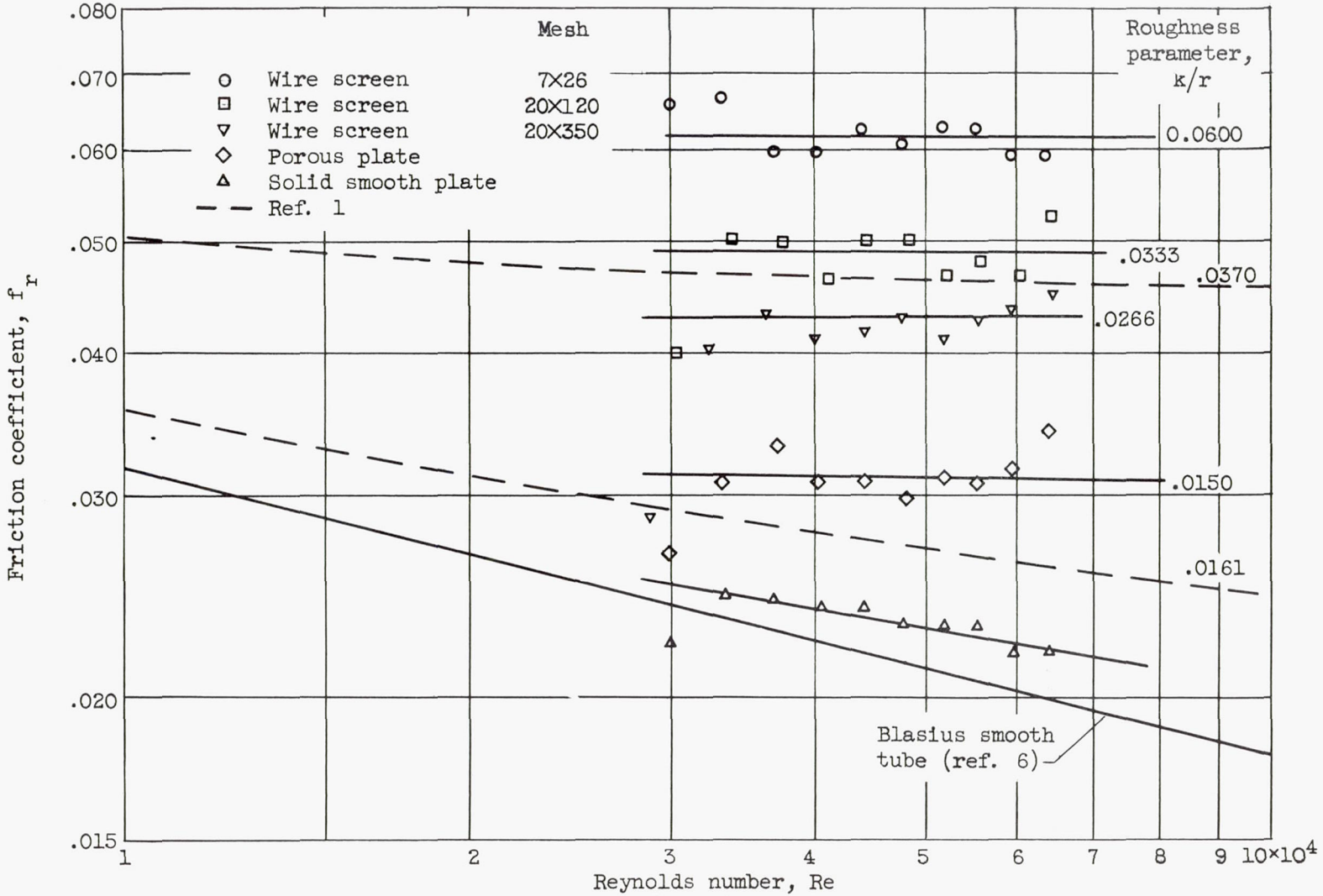

Figure 14. - Friction coefficients for lower wall of channel without air injection compared with available data.

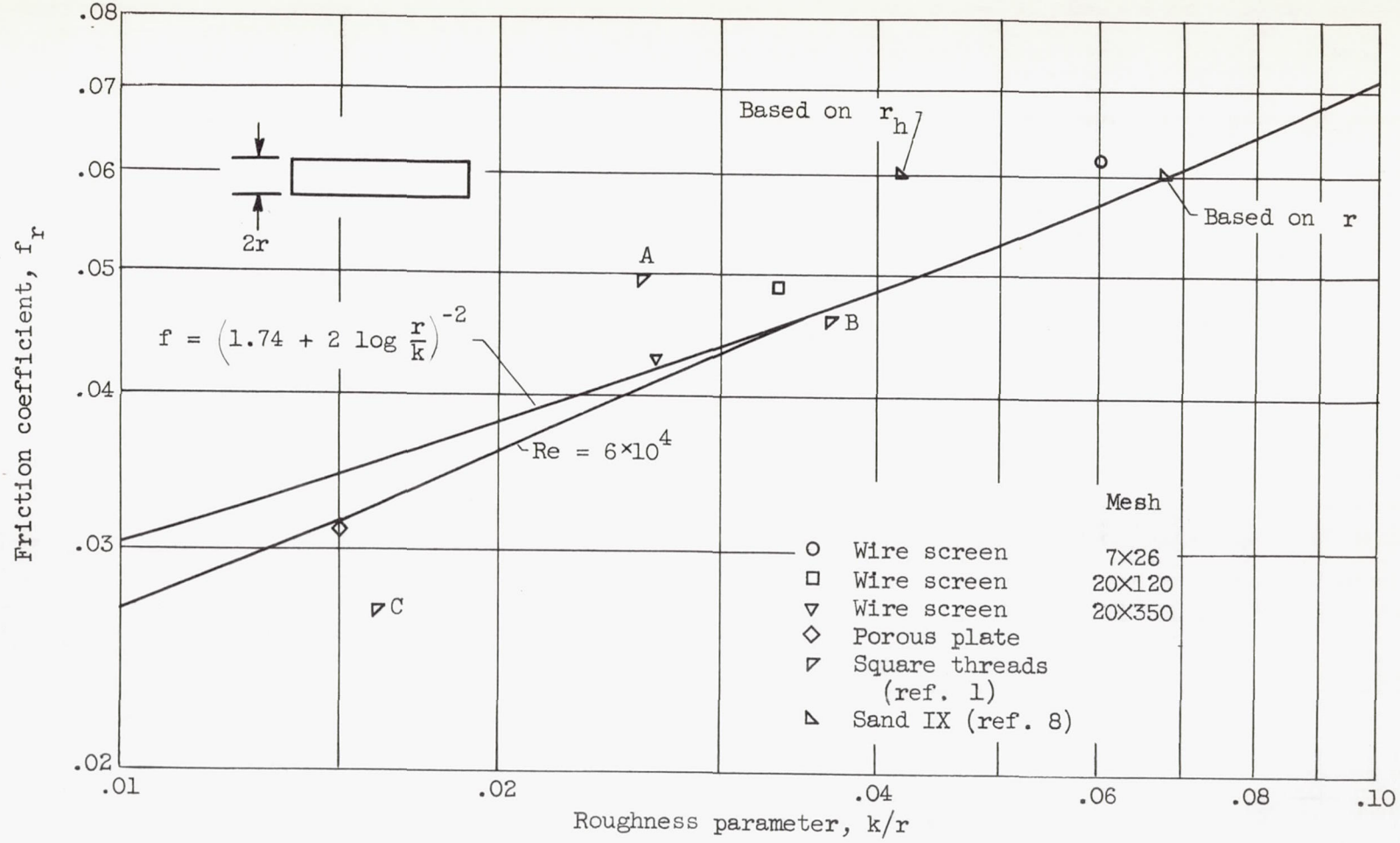

Figure 15. - Friction coefficients for various roughnesses.

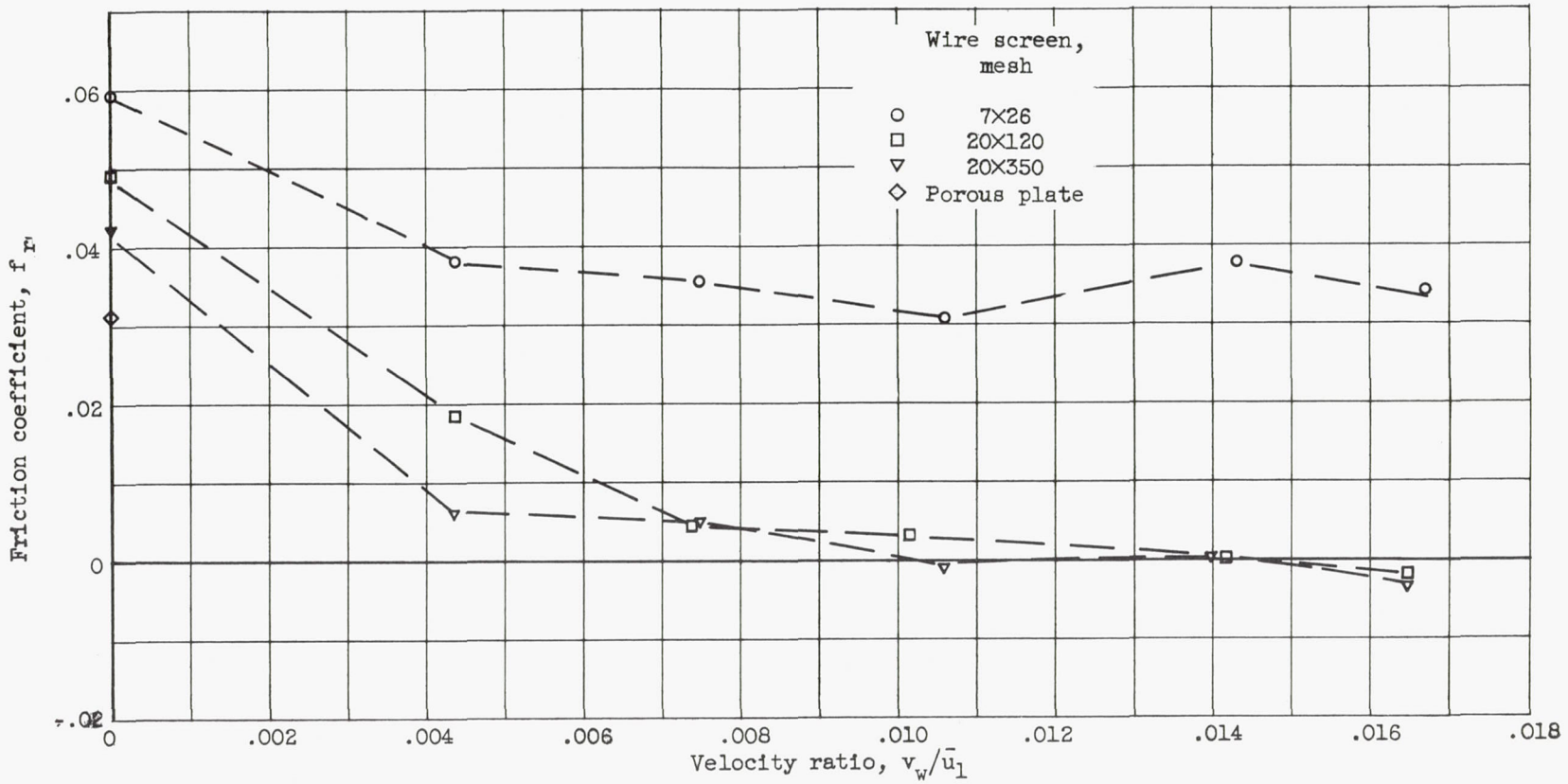

Figure 16. - Friction coefficients for porous rough surfaces as determined from channel data. Reynolds number, 6×10^4.

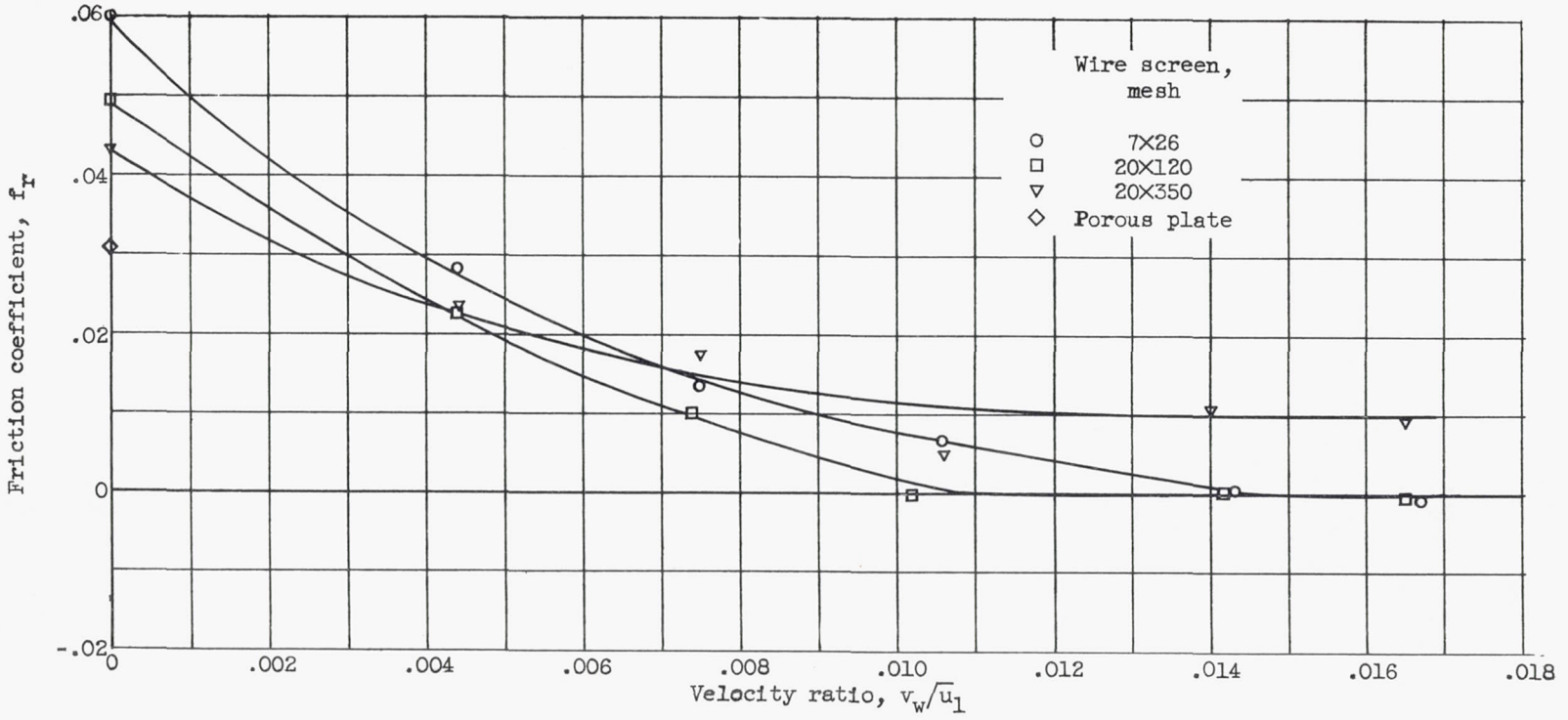

Figure 17. - Friction coefficients for porous rough surfaces with momentum change correction. (Based on 20×120 screen run.)